DOI: 10.1021/ma101235j

Macromolecules
ARTICLE

In Situ and Time-Resolved Small-Angle Neutron Scattering Observation of Star Polymer Formation via Arm-Linking Reaction in Ruthenium-Catalyzed Living Radical Polymerization[1]

Takaya Terashima,*,† Ryuhei Motokawa,*,‡ Satoshi Koizumi,*,‡ Mitsuo Sawamoto,*,† Masami Kamigaito,§ Tsuyoshi Ando,†,∥ and Takeji Hashimoto‡

†*Department of Polymer Chemistry, Graduate School of Engineering, Kyoto University, Katsura, Nishikyo-ku, Kyoto 615-8510, Japan,* ‡*Research Group for Soft Matter & Neutron Scattering, Advanced Science Research Center, JAEA, Ibaraki 319-1195, Japan, and* §*Department of Applied Chemistry, Graduate School of Engineering, Nagoya University, Furo-cho, Chikusa-ku, Nagoya 464-8603, Japan.* ∥*Present address: Graduate School of Material Science, Nara Institute of Science and Technology, 8916-5 Takayama-cho, Ikoma, Nara 630-0192, Japan*

Received June 2, 2010; Revised Manuscript Received August 12, 2010

ABSTRACT: *In situ* and time-resolved small-angle neutron scattering (SANS) was employed for the elucidation of star polymer formation mechanism via linking reaction of living linear polymers in ruthenium-catalyzed living radical polymerization. Here, methyl methacrylate (MMA) was first polymerized with R−Cl/$RuCl_2(PPh_3)_3$/tribuylamine (*n*-Bu_3N) initiating system, followed by the addition of ethylene glycol dimethacrylate (EGDMA: **3**) as a linking agent. After the *in situ* addition of a small amount of **3** to living linear PMMA, the SANS analysis revealed the following three steps: (process II-1) formation of block copolymers (**4**) and competitive formation of the small star polymers via the linking reaction of **4** and **4**; (process II-2) star−star linking of the small star polymers into star polymers and putting **4** into the core of the star polymers, leading to formation of the microgel-core star polymers; (process II-3) growth of the microgel-core star polymers (**5**) via placement of **4** into the microgel-core star polymers. Furthermore, the SANS profiles, obtained as a function of polymerization time, were quantitatively analyzed with a core−shell spherical model in order to determine the microstructures of the star polymers: The final reaction product had an average radius of microgel-core (∼1 nm), and average arm numbers $N \sim 17$.

1. Introduction

Star or star-shaped polymers[2−10] are synthesized by living polymerizations[5−10] with key compounds such as multifunctional initiators or terminators, or divinyl compounds, which link the terminal of linear living polymer chains. While the former two methods based on multifunctional initiators or terminators with an accurate number of functional groups can afford star polymers with the desired number of arm chains, the latter with divinyl compounds as linking agents of linear polymers results in distributed numbers of arm chains due to statistically occurring linking reactions. However, the linking method can produce star polymers with a large number of arm chains (10−100) and consists of relatively simple procedures just by adding a small amount of divinyl compounds into living polymer solutions after most of vinyl monomers for the arm chain constituents are consumed. This method is more practical than the former two methods, which require the complicated synthesis of the multifunctional agents, and is expected to be useful for various applications.

The star polymer synthesis based on the linking reaction was first developed in a living anionic polymerization of nonpolar monomers like styrene and dienes combining with divinylbenzene (DVB).[2,5,11−13] The effects of the reaction conditions on the star polymer yield, size of the star polymers, number of arm chains, etc. were investigated to efficiently characterize the products. Especially, kinetic experiments[14] and UV−vis spectroscopic study[12b] turned out to be powerful tools to clarify the linking mechanism of linear polymers for star polymer formation. Living anionic polymerization characteristically performs reaction selectivity between two vinyl groups in a DVB monomer; reaction rate constant of the pendant vinyl group in block copolymers with an anionic polymer terminal is approximately 10 times smaller than that of two vinyl groups in DVB monomer.[5,14] Therefore, diblock copolymerization and cross-linking process are distinctly separated to each other after addition of a linking agent into a living prepolymer.[5] Typically, living anionic polymerization of DVB from a polystyryl lithium (PStLi) first proceeds to give diblock copolymers of styrene and DVB with dangling olefins, and subsequently, the diblock copolymers start to coagulate by cross-linking the pendant vinyl groups. On the other hand, living radical polymerization,[7−10] similar to living cationic polymerization,[6] hardly exhibits reaction selectivity. Thus, diblock copolymerization and cross-linking among block copolymers with dangling vinyl groups would occur competitively.

The distinctive property of such star polymers would be a low viscosity in comparison to the linear polymers with similar molecular weight due to the smaller radius of gyration and thereby the smaller degree of the chain entanglements,[2] while any other special properties related to their functions may have not been observed until the developments of living polymerizations of polar and/or functional monomers. However, recent remarkable progresses in living anionic,[3] cationic,[6,15] and radical[7,16−19] polymerizations have enabled the preparation of various star polymers carrying functional moieties.

*Corresponding authors.

 Published on Web 09/14/2010 © 2010 American Chemical Society

One of our groups has developed and employed the ruthenium-catalyzed living radical polymerization,[7,20] which is versatile for various vinyl monomers and highly tolerant to polar functional groups,[21−24] for the star polymer synthesis with linking agents of divinyl compounds.[7c,d,16b,d,17] We have thus already shown that the ruthenium-catalyzed system is effective in preparing a wide variety of star polymers that possess polar functional groups, not only in the arm chains[17c] and at the surfaces,[16d] but also in the microgel-cores,[16b] into which we can introduce even metal moieties via coordination based on the functional substituents.[17] These novel functionalized star polymers exert special properties owing to the unique structures.[17,25] In addition to such functionalizations, we have deeply characterized the structures of the isolated star polymers by various analytical methods including NMR,[16a−d,17] size-exclusion chromatography (SEC) equipped with multiangle laser light scattering (SEC−MALLS),[16a,b,d,e,17] small-angle X-ray scattering (SAXS),[16e] atomic force microscopy (AFM),[17] and transmission electron microscopy (TEM).[17a,b] They provided information on the star polymers, such as absolute molecular weights, number of arm chains, radius of gyration, shape, and total and core sizes. The linking mechanism, through competitive reactions between block copolymerization of a divinyl compound and linking reaction of the obtained block copolymers, were sufficiently clarified by time-resolved SEC and ^{1}H NMR analyses of isolated polymers.[16,17] However the detailed time-evolution processes of the star polymer formation, such as the process on how the linear polymers get together to form the microgel-cores, has not been fully elucidated, because of the difficulty in the direct *in situ* analysis of the process.

On the other hand, another of our groups has employed time-resolved small-angle neutron scattering (SANS) for the *in situ* observation of the time-evolution of the molecular building-up process and the molecular self-assembling process in living anionic and radical polymerizations.[26,27] Time-resolved SANS measurement is one of the most powerful techniques for the direct analysis of reaction systems, because the low energy of cold neutrons (∼meV) is extremely important to avoid the radiation-induced side-reactions in reaction systems of our interest.[26−28] Because of high transmittance of neutrons for sample specimens, *in situ* and time-resolved SANS measurement has enabled us to directly examine the reaction solution enclosed in the quartz cell and quantitatively determine molecular characteristics of propagating living polymers and/or molecular self-assembly during living anionic polymerization[26,28] or living radical polymerization.[27]

Herein, this paper is directed to the *in situ* and time-resolved SANS analysis of star polymer formation via the linking reaction with divinyl compounds in ruthenium-catalyzed living radical polymerization. In particular, length scales covered by SANS are from 1 to 100 nm, which appropriately match sizes of the microgel-core star polymers and their spatial arrangement in the solution. Furthermore, the simultaneous multianalyses of aliquots of the reaction solutions taken at varying reaction times by SEC, SEC−MALLS, and NMR, together with the in situ time-resolved SANS, will provide us more complete information on the star polymer formation.

Along the lines as described above, we investigated two polymerization solutions: solution A with optimized reaction condition and solution B with high monomer concentration. As shown in Scheme 1 commonly for both of the solutions, we first polymerized methyl methacrylate (MMA) by the ruthenium-mediated initiating system to obtain well-defined linear living polymers (**2**) as reaction process I, followed by direct addition of ethylene glycol dimethacrylate (EGDMA: **3**) as a linking agent to form microgel-core star polymers (**5**) as reaction process II. The in situ and time-resolved SANS analyses of solution A allowed us to determine the time-evolution of core size (R_{core}),

Scheme 1. Synthetic Route of the Microgel-Core Star Polymers via the Arm-Linking Reaction Method in Ruthenium-Catalyzed Living Radical Polymerization

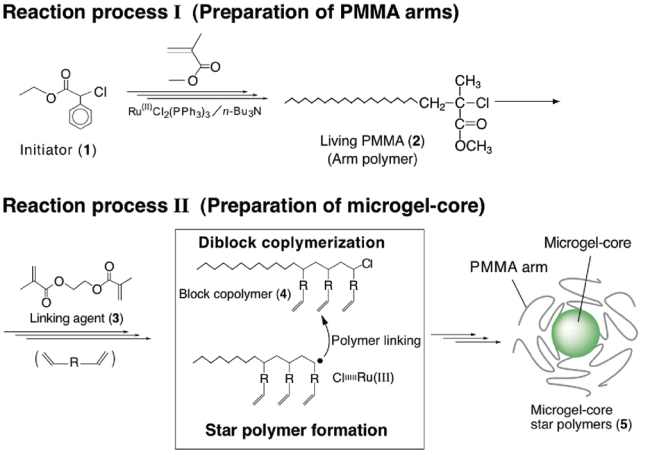

number of arm chains per core (N_{SANS}), number density of cores (n), and the hard sphere radius of microgel-core star polymer (R_h) in the course of polymerization. These results enabled us to quantitatively clarify the detailed mechanism in reaction process II for the first time. In addition, we discuss macroscopic gelation, which is clearly observed for the condensed reaction solution B in reaction process II. To the best of our knowledge, this is the first report on the direct observation of microgel-core star polymer formation process via living radical polymerization.

2. Experimental Section

2.1. Materials. MMA was from a commercial source (Tokyo Kasei; purity >99%), dried overnight over calcium chloride, and purified by double distillation from calcium hydride before use. Ethyl-2-chloro-2-phenylacetate (ECPA: **1**; initiator) was prepared according to the literature.[29] EGDMA (Aldrich; purity >98%) was purified by distillation from calcium hydride before use. $RuCl_2(PPh_3)_3$[20] (Aldrich; purity >97%) was used as received and handled in a groove box under a moisture- and oxygen-free argon atmosphere (H_2O < 1 ppm, O_2 < 1 ppm). Tributylamine (n-Bu_3N)[30] (Tokyo Kasei; purity >98%) was bubbled with dry nitrogen for more than 15 min before use. Internal standards [n-octane, Wako, purity >98%; tetralin (1,2,3,4-tetrahydronaphthalene), Kisida Chemical, purity >98%] for gas chromatography (n-octane for MMA; tetralin for EGDMA) were dried overnight over calcium chloride and distilled twice from calcium hydride. Toluene-d_8 (CIL; deuterium >99.5%) was dried overnight over molecular sieves 4A (Wako) and degassed by reduced pressure before use.

2.2. Preparation of Polymerization Solution. In this study, we prepared two different polymerization solutions, solution A and solution B, with different MMA concentration of 2.0 and 6.0 M, respectively, keeping the same molar ratio of a monomer, a linking agent, and an initiator: [MMA]/[**3**]/[**1**] (= 100/10/1) (see Table 1). Solution A is an optimized condition to prepare the microgel-core star polymers in high yield,[16,17] whereas solution B is a high monomer concentration condition used to intentionally produce the so-called "*star−star coupling*" and/or the macroscopic gelation.

Solution A for time-resolved SANS measurements coupled with the molecular analyses with SEC, SEC−MALLS, and NMR measurements was first prepared according to the following method: in a glass tube (50 mL), first placed with $RuCl_2(PPh_3)_3$ (0.1 mmol, 95.7 mg) and kept at 25 °C under dry nitrogen, we sequentially added toluene-d_8 (6.43 mL), n-octane (0.2 mL), n-Bu_3N (0.4 mmol, 1.0 mL, 400 mM in toluene-d_8), MMA (20 mmol, 2.11 mL), and **1** (0.2 mmol, 0.25 mL, 801 mM in toluene-d_8) (final reaction solution: 10 mL). Note that

Table 1. Solution A and B for Time-Resolved SANS Observation of Star Polymer Synthesis in Ru(II)-Catalyzed Living Radical Polymerization

	$[MMA]_0$ (M)	$[1]_0$ (mM)	$[RuCl_2(PPh_3)_3]_0$ (mM)	$[n\text{-}Bu_3N]_0$ (mM)	$[3]_{add}$ (mM)
solution A [Reaction process I][a]	2.0	20	10	40	0
solution A [Reaction process II][b]	1.3	13	6.7	27	130
solution B [Reaction process I][a]	6.0	60	10	40	0
solution B [Reaction process II][b]	4.0	40	6.7	27	400

[a] Prepolymer solution for reaction process I (arm): $[MMA]_0/[\mathbf{1}]_0/[RuCl_2(PPh_3)_3]_0/[n\text{-}Bu_3N]_0$ in toluene-d_8 at 80 °C. [b] Final concentration in reaction process II after in situ addition of a linking solution (solution A, $[\mathbf{3}]_{add}$ = 400 mM in toluene-d_8; solution B, $[\mathbf{3}]_{add}$ = 1200 mM in toluene-d_8) into a prepolymer solution (prepolymer solution/linking solution = 2/1, v/v).

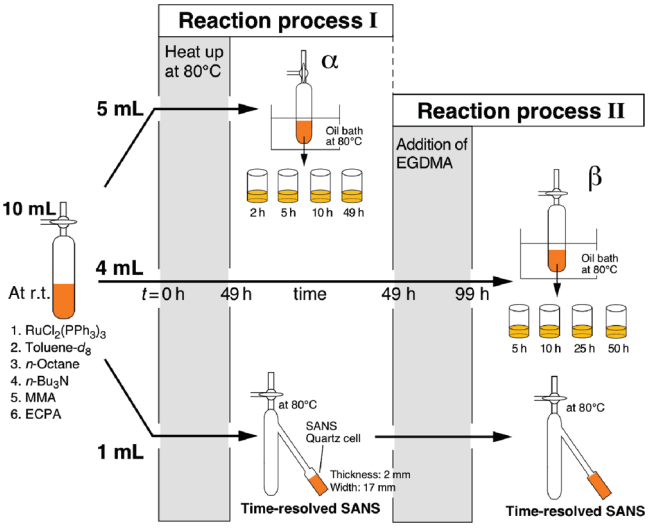

Figure 1. Experimental procedures of the *in situ* and time-resolved SANS observation for the synthesis of microgel-core star polymers.

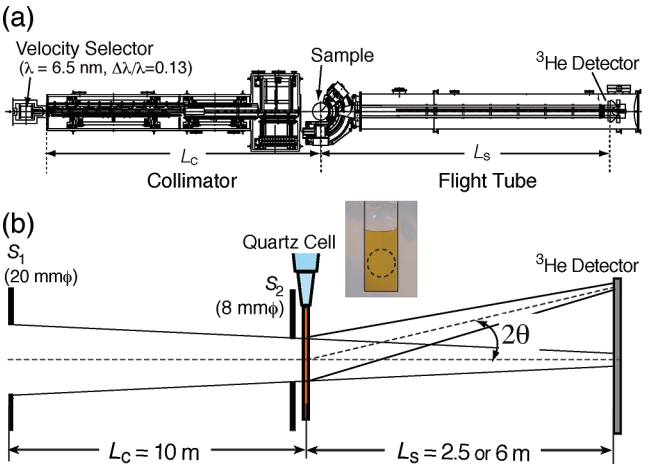

Figure 2. Schematic diagrams of (a) SANS spectrometer and (b) its pinhole SANS geometry, employed in this study.

toluene-d_8 was used as a solvent for SANS, in order to obtain a sufficient scattering contrast between the polymer and solvent.

The reaction solution (10 mL) was distributed into three different vessels as shown in Figure 1. For time-resolved SANS measurements, we employed a quartz cell connected to the glass tube with a three-way stopcock, where the thickness and width of the cell are 2 mm and 17 mm, respectively. By a syringe technique under dry nitrogen, the quartz cell was filled with the prepolymerization solution ($RuCl_2(PPh_3)_3$/*n*-octane/*n*-Bu_3N/MMA/**1**) in toluene-d_8 of 1.0 mL. Additionally, two glass tubes (α and β shown in Figure 1) were prepared to analyze molecular weight and molecular weight distribution of the products and monomer conversion. The glass tube α with 5 mL of the solution is for monitoring reaction process I (arm synthesis) by the sampling at predetermined periods, whereas the glass tube β with 4 mL is for monitoring reaction process II (star polymer synthesis) after *in situ* addition of a linking agent (**3**). As for solution B, we followed the experimental procedure described above for solution A.

2.3. In situ Observation of Polymerization Process by SANS and Molecular Analyses. To initiate MMA polymerization in the quartz cell for *in situ* SANS analysis and in the glass tubes (α and β) for molecular analyses, we simultaneously placed the glass tubes and the quartz cell in an oil bath or in heater block controlled at 80 °C, respectively. Time-resolved SANS measurement in reaction process I was performed immediately after the initiation of the reaction in a quartz cell, along with monitoring the polymerization by the sampling from the glass tube α at predetermined periods. The sampled solutions were terminated by the cooling at −78 °C and were analyzed by GC and SEC to determine monomer conversion, number-averaged molecular weight (M_n), and M_w/M_n, characterizing molecular weight distribution (MWD), where M_w is the weight-averaged molecular weight.

Before the arm-linking reaction, we prepared the following linking agent solution: EGDMA (**3**) (0.60 mL, 2000 mM in toluene-d_8) and tetralin (0.06 mL) in toluene-d_8 (total: 3.0 mL). When the MMA conversion reached over ca.90%, the linking agent solution of 2 and 0.5 mL was directly added into the glass tube β and the quartz cell through the syringe under inert atmosphere to start the linking reaction of poly(MMA) arms (reaction process II) respectively. Reaction process II in the quartz cell was subsequently monitored by time-resolved SANS without termination, as well as that in the glass tube β by the sampling at the predetermined times for molecular analyses.

2.4. SANS Spectrometer. SANS measurements were performed by SANS-J-II spectrometer installed at the research reactor JRR-3 (20 MW), Japan Atomic Energy Research Agency (JAEA), at Tokai, Japan.[31] With a velocity selector, cold neutron was monochromatized so that wavelength λ = 0.65 nm and the wavelength distribution $\Delta\lambda/\lambda$ = 0.13. SANS-J-II is composed of the following two vacuum chambers as shown in Figure 2a: (i) a T-shape collimator at an upper stream of the sample position, in which the pinhole collimators were installed, and (ii) a flight tube after the sample position, in which the ^{3}He position sensitive detector (0.58 m diameter and 5 mm resolution) was placed at the distance L_S from the sample. A conventional pinhole collimation with the first and second collimator sizes being S_1 and S_2 = 20 and 8 mm ϕ was used, respectively, as shown in Figure 2b. The quartz cell enclosing the reaction solution was set behind a second pinhole S_2. Two sample-to-detector distances were set in our SANS experiment; one L_S = 6 m, covering the q-range of $0.055 < q\,(nm^{-1}) < 0.5$ and the other L_S = 2.5 m, $0.15 < q\,(nm^{-1}) < 1.65$, respectively, where $q = (4\pi/\lambda)\sin(\theta)$ is the magnitude of the scattering vector **q** with scattering angle 2θ and λ. The scattering data recorded with the 2-dimensional detector were corrected for counting efficiency, instrumental background, and air scattering, according to a pixel-to-pixel method. After circularly averaging the SANS intensity distribution, we converted the scattering to the absolute intensity units (cm^{-1}) using a secondary standard of an irradiated Al plate. Incoherent scattering from hydrogen, estimated from incoherent scattering intensity for a reference sample (toluene-h_8), was subtracted from the net absolute intensity. The corrected scattered intensity distribution is designated as $I(q)$ hereafter.

2.5. Apparatus for Molecular Characterization. M_n, M_w/M_n, and MWD curves of the polymers were measured by SEC in $CHCl_3$ at 40 °C on three linear-type polystyrene gel columns (Shodex K-805 L; flow rate = 1 mL/min; exclusion limit = 5×10^6; pore size = 20−1000 Å; 0.8 cm i.d. × 30 cm) that were connected to a Jasco PU-980 precision pump and a Jasco RI-930 refractive index detector. The columns were calibrated against 12 standard PMMA samples (Polymer Laboratories; M_n = 630−1 200 000; M_w/M_n = 1.06 - 1.22). The monomer conversions were determined from the concentration of residual monomers against internal standards, measured by gas chromatography (GC: Shimadzu GC-8A) equipped with a packed column (MMA, PEG-1500, 2.1 m × 3.2 mm, Shimadzu; EGDMA (**3**), silicon DC11, 2.1 m × 3.2 mm, Shimadzu). ^{1}H NMR spectra were recorded in CD_2Cl_2 at 25 °C on a JEOL JNM-LA500 spectrometer, operating at 500.16 MHz. Polymer samples for ^{1}H NMR analysis were fractionated by preparative SEC (column: Shodex K-5002F). The absolute weight-average molecular weight and mean radius of gyration (R_g) of obtained polymers were evaluated by multiangle laser light scattering coupled with SEC (SEC−MALLS) in $CHCl_3$ at 40 °C on a Dawn E instrument (Wyatt Technology; Ga−As laser, λ = 690 nm in air; the range of scattering angle is covered from 20 to 153° in air). The refractive index increment (dn/dc) was measured in $CHCl_3$ at 40 °C on an Optilab DSP refractometer (Wyatt Technology; λ = 690 nm, c < 2.0 mg/mL).

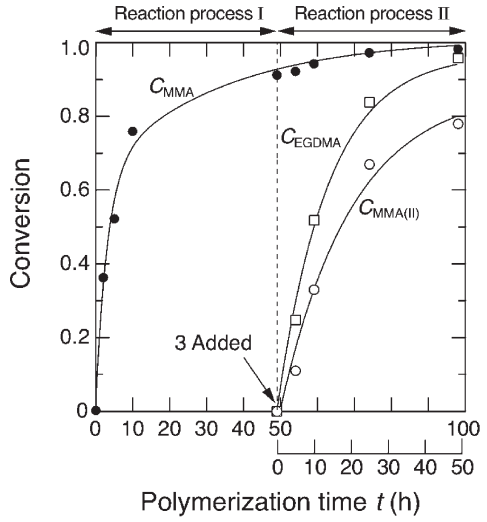

Figure 3. Conversion of MMA (C_{MMA}; filled circles) in the whole reaction processes I and II as a function of total polymerization time and the conversion of EGDMA (C_{EGDMA}; open squares) and MMA ($C_{MMA(II)}$; open circles) in reaction process II as a function of polymerization time t in reaction process II.

3. Results

3.1. Molecular Analyses (SEC, GC, and NMR): Solution A. *3.1.1. Reaction Process I (Arm Polymers).* On the basis of the previously optimized condition of solution A (see Table 1),[16,17] methyl methacrylate (MMA) was first polymerized with a ruthenium complex $[RuCl_2(PPh_3)_3]$[20,16,17] as a catalyst coupled with a chloride initiator (**1**, ECPA)[29] and an amine additive (n-Bu_3N)[30] in toluene-d_8 at 80 °C, in the glass tube α, β, and the SANS quartz cell. Aliquots of the polymerization solution in the glass tube α were sampled in the predetermined periods (2, 5, 10, 49 h) as illustrated in Figure 1, and the solution was analyzed by GC for the determination of monomer conversion of MMA, $C_{MMA}(t)$, (Figure 3). The monomer was smoothly consumed to reach 91% conversion in 49 h.

The aliquots were also evaluated by SEC and/or SEC−MALLS for molecular weight and MWD and by ^{1}H NMR for polymer structure. Figure 4a shows the time-evolution of the SEC chart of solution A obtained in reaction process I. We observed a peak originating from the PMMA arms during the course of reaction process I, where the peak gradually shifts toward higher molecular weight region and becomes sharp as the polymerization proceeds, indicating that the molecular weight distribution becomes narrower

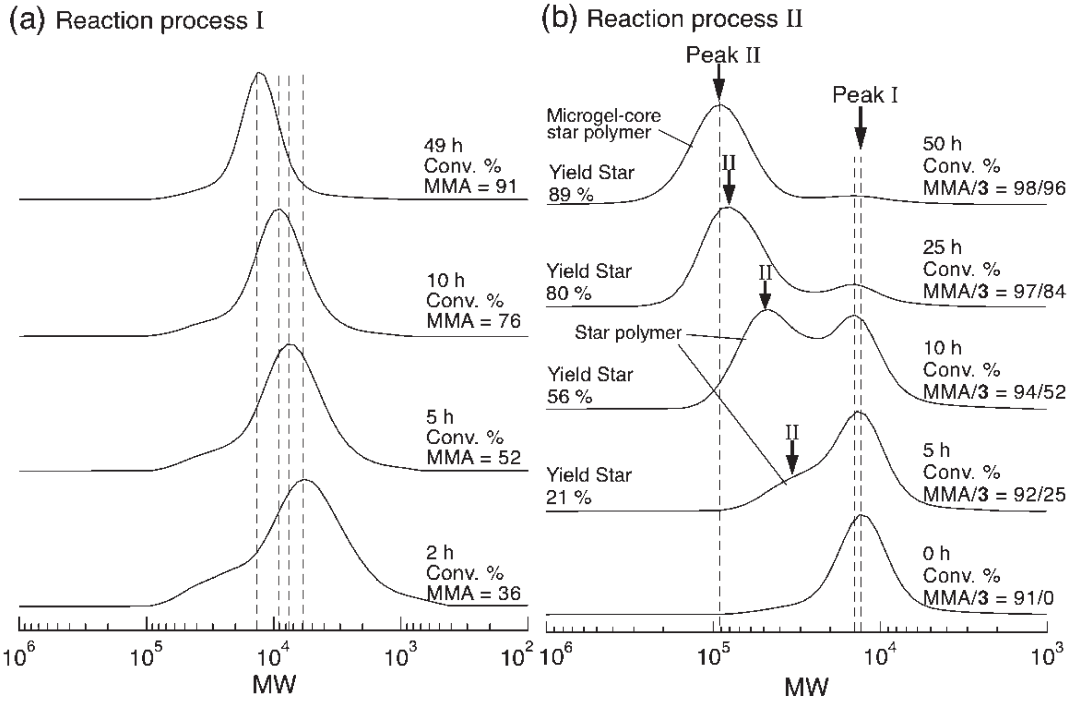

Figure 4. SEC data obtained at polymerization times in (a) reaction process I and (b) reaction process II. The broken lines show the peak position of peak I in reaction processes I and II, while the arrows show the peak positions of peak II at a given t. C_{MMA} (%) obtained in reaction process I and C_{MMA}/C_{EGDMA} and the yield of the microgel-core star polymers obtained in reaction process II are described on each side of the SEC data.

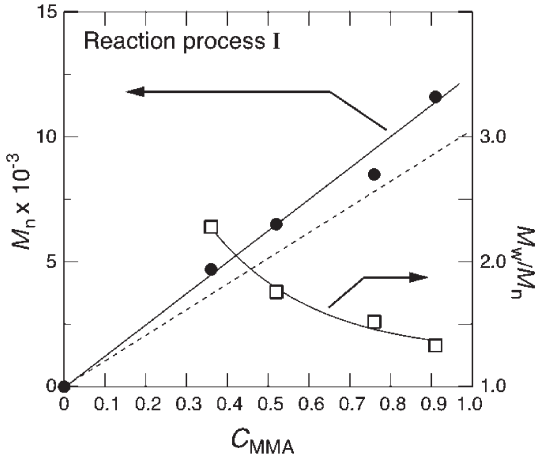

Figure 5. Number-averaged molecular weight M_n (filled circles) and polydispersity index M_w/M_n (open squares) of PMMA arms obtained in reaction process I as a function of C_{MMA}. The dashed line is a calculated molecular weight, based on the data shown in Table 1 for solution A.

with increasing $C_{MMA}(t)$ (see Figure 5). The M_n of the obtained polymers increased in direct proportion to $C_{MMA}(t)$, and was close to the calculated value (shown by the broken line), assuming that one molecule of initiator generated one living polymer chain (Figure 5), finally leading to living PMMA arms (**2**) with controlled M_n and relatively narrow molecular weight distribution (M_n = 11600, M_w/M_n = 1.33).

3.1.2. Reaction Process II (Star Polymers). At the 91% conversion of MMA in the glass tube α of solution A ([remained MMA] ~ 200 mM), the toluene-d_8 solution of a linking agent EGDMA (**3**) (feed ratio of **3** to **1**: [**3**]/[**1**] = 10/1)[16,17] was then directly and simultaneously added into the glass tube β and the SANS quartz cell, both of which contain the living PMMA arm (**2**) solution (M_n = 11600, M_w/M_n = 1.33, Conv. 91%), to induce the linking reactions (reaction process II). In reaction process II, aliquots of the polymerization solution in the glass tube β were sampled at 5, 10, 25, and 50 h, as illustrated in Figure 1, in order to evaluate the molecular weight of the products and the conversion of the monomers by means of SEC and GC. It should be noted that, in the fresh feed of EGDMA, the concentration of the remaining MMA is almost equal to that of the EGDMA. In Figure 3, the monomer conversions of EGDMA and MMA in reaction process II, $C_{EGDMA}(t)$ and $C_{MMA(II)}(t)$, are plotted as a function of t. EGDMA and MMA were concurrently consumed, demonstrating that random copolymerization of MMA and EGDMA occurs from the growing terminal of **2** because of their similar reactivity for growing radicals.

Figure 4b shows SEC of the obtained polymers during the reaction process II in solution A. The samples obtained after t = 5 h exhibited a bimodal SEC curve consisting of peaks I and II. Peak I slightly shifted to higher molecular weight region as the reaction proceeded, though the peak position is almost unaltered at $t \gtrsim 5$ h. Obviously, peak I showed slightly higher molecular weight than that of PMMA arms (**2**), suggesting formation of block copolymers (**4**) of PMMA and a short random copolymer comprising of MMA and EGDMA segment [poly(MMA-*ran*-EGDMA)].[16a] The steady peak position observed at $t \gtrsim 5$ h indicates that the apparent molecular weight of the poly(MMA-*ran*-EGDMA) is almost constant for $t \gtrsim 5$ h, because of competing reactions between the linear growth of the copolymer sequence and its linking reaction into star polymers, as will be detailed below.

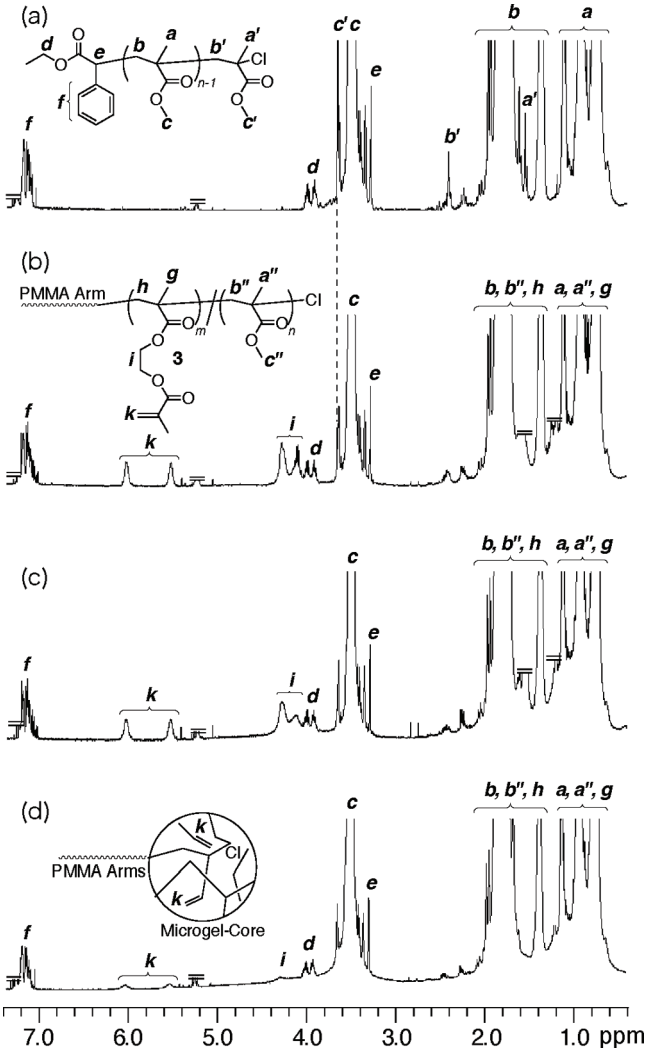

Figure 6. ^{1}H NMR spectra (in CD_2Cl_2 at room temperature) obtained during the synthesis of microgel-core star polymers: (a) PMMA arms **2**; (b–d) the products obtained at t = 5, 10, and 50 h in reaction process II.

Peak II, in turn, obviously showed higher molecular weight than that of **4**, attributed to the small star polymers obtained from the intermolecular cross-linking reaction of the block copolymers (**4**). Peak II gradually shifted to higher molecular weight region and the yield increased as the reaction proceeded, finally led to the microgel-core star polymers (**5**) in high yield (90%) at 50 h (total polymerization time: 99 h). Characterized by SEC–MALLS, **5** had M_w of 3.4 × 10^5, average arm numbers per a star polymer ($N_{SEC-MALLS}$) of 17,[32] and an overall radius of gyration (R_g) of 8.1 nm.[16e]

The increment of the apparent molecular weight $\Delta M_{app,I}$ in reaction process II was estimated from the peak position of peak I, where $\Delta M_{app,I}$ is defined by

$$\Delta M_{app,I} = M_I - M_{PMMA,arm} \quad (1)$$

where M_I is the apparent molecular weight of the reaction product estimated from the peak position of peak I, while $M_{PMMA,arm}$ (= 13210) is that of PMMA chains at the end of reaction process I. $\Delta M_{app,I}$ thus estimated increased up to ~970 at C_{EGDMA} = 0.52 and $C_{MMA(II)}$ = 0.33 (corresponding to t = 10 h) and then almost kept this value at t > 10 h, indicating that the average number of the monomeric unit (DP) of poly(EGDMA-*ran*-MMA) block chains reaches a constant value of ~6.5 at the early stage of reaction process II, where the average molecular weight of EGDMA and

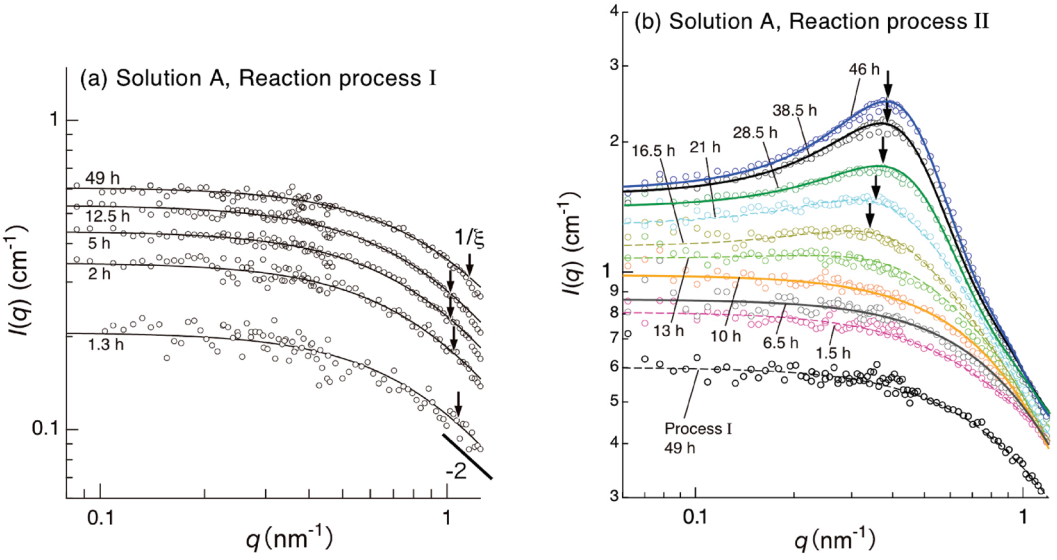

Figure 7. *In situ* and time-resolved SANS profiles of solution A at varying polymerization time t obtained in (a) reaction process I and (b) reaction process II. The profiles shown by circles and solid lines indicate the experimental and theoretical scattering profiles. The theoretical scattering profiles in reaction process I were reproduced by the Ornstein−Zernike theory (eq 2), and those in reaction process II at t = 6.5 and 10 h and at t = 28.5 to 46 h were reproduced by eq 14 and 16, respectively. The dashed lines described on the SANS profiles of reaction process II are guides for the eyes.

MMA [(198.22 + 100.12)/2] was used to calculate $DP \sim 6.5$. Poly(EGDMA-*ran*-MMA) hardly grow larger than the average $DP \sim 6.5$, even though further monomers are consumed, probably because the grown block copolymers are preferentially incorporated into the linking reaction.

The polymers obtained during reaction processes I and II were analyzed by ^{1}H NMR (Figure 6). PMMA arms (**2**), finally obtained from the process I in t = 49 h, exhibited the signals originating from the protons of the terminal MMA unit adjacent to ω-terminal chlorine (a′, 1.5 ppm; b′, 2.4 ppm; c′, 3.7 ppm) and those of initiator **1** (d, 3.9−4.0 ppm; e, 3.3 ppm; f, 7.1−7.2 ppm), along with the characteristic signals of a PMMA (a, 0.7−1.2 ppm; b, 1.3−2.0 ppm; c, 3.4−3.6 ppm) (Figure 6a). The DP was estimated as 113 from the signal intensity ratio of initiator to main chain [(c/3)/(d/2)], thus resulting in 11500 of the M_n (NMR) according to the following equation: 198.6 (F_w of **1**) + 100.12 (F_w of MMA) × DP. The M_n (NMR) in by ^{1}H NMR was in good agreement with those by SEC [M_n (SEC) = 11600]. Thus, the number-average α-end functionality (F_n) for the initiator fragment, obtained from M_n (SEC)/M_n (NMR), was close to unity (1.02),[33] also supporting the conclusion that this system induced living polymerization of MMA to achieve an efficient linking reaction.

At t = 5 h after addition of EGDMA (Figure 6b), the peaks of vinyl protons (k: 5.5, 6.2 ppm) and methylene protons (i: 4.0−4.3 ppm) derived from EGDMA were observed, whereas the peak of PMMA terminal unit (c′) completely disappeared. These changes indicated that EGDMA and MMA residue react with the living end of prepoly(MMA) (PMMA arms) to give a block copolymers (**4**) carrying a short linear random segment of EGDMA and MMA.[16,17] At t = 10 h after addition of EGDMA (Figure 6c), the peaks of vinyl protons (k: 5.5, 6.2 ppm) and methylene protons (i: 4.0−4.3 ppm) were slightly broader than those at 5 h, indicating that star polymers with small number of arms are gradually forming between t = 5 to 10 h. In the final products (Figure 6d), the vinyl protons (k) and the methylene counterparts (i) were quite broad and almost disappeared, corresponding to the formation of microgel-core network with EGDMA and MMA.[16,17]

3.2. Time-Resolved SANS Observations: Solution A. Figure 7a shows the time-evolution of $I(q, t)$ obtained from reaction process I in solution A. All the scattering profiles $I(q, t)$s are well reproduced by the Ornstein−Zernike (OZ) formalism,[34] as shown by the best-fitted theoretical profiles (solid lines), which will be discussed later in conjunction with eq 2 in section 4.1. As the polymerization proceeds, the scattering intensity gradually increased and the characteristic q value, q^*(= 1/ξ, ξ will be defined later), simultaneously shifted toward lower q up to 12.5 h as indicated by thick arrows in Figure 7a. On the contrary, after t = 12.5 h, q^* slightly shifted toward higher q, because PMMA arm concentration (C) exceeds the overlap concentration (C^*), defined as $C^* = 3M_n/(4\pi N_A R_g^3)$, where N_A is an abogadro constant.[35] Details of the scattering behaviors will be discussed later in conjunction with Figure 9. These results indicate that the PMMA arms grow in molecular weight and homogeneously dissolved in the matrix of MMA and toluene-d_8 during reaction process I.

Figure 7b shows time-resolved SANS profiles obtained for solution A in reaction process II. Until t = 10 h, the scattering intensity gradually increased as the reaction proceeded, keeping a q-dependence given by the OZ formalism.[34] At $t \gtrsim$ 16.5 h, we start to recognize a broad scattering maximum appeared at around q = 0.32 nm^{-1}. The maximum intensity kept remarkably increasing with t, whereas the q-value at the maximum intensity (q_m) slightly increased from ∼0.32 to ∼0.39 nm^{-1}. The scattering maximum observed in this solution is originated from interparticle interference among the star polymers and/or microgel-core star polymers. At t = 46 h, the characteristic distance among the microgel-core star polymers ($2\pi/q_m$) was determined as ∼16 nm.

3.3. Time-Resolved SANS Observations: Solution B. In sharp contrast to solution A, solution B with high monomer concentration ([MMA]$_0$ = 6.0 M) involved fast consumption of MMA (reaction process I) to give PMMA arms with controlled molecular weight (M_n = 10500; M_w/M_n = 1.74; conversion 87%; 12 h). Subsequently added EGDMA (**3**) into the solution was also consumed quite fast for the linking reaction within the next 12 h (reaction process II: total conversion MMA/**3** = 99/99%). The solutions in glass tube β after t = 8 h in reaction process II formed a macroscopic gel, while the solutions after t = 4.5 and 5.5 h were still fluid and had coexistence of sol and gel components.

The SANS profiles in reaction process I were also characterized by the OZ formalism similarly to solution A. After

the addition of EGDMA (reaction process II), the overall scattering intensity increased as the linking reaction proceeded (Figure 8). At $t = 3.5$ h, a broad scattering maximum started to appear around $q_m = 0.4$ nm^{-1}, and at $t \gtrsim 8$ h, the SANS profiles showed shoulder peaks at $q > 1$ nm^{-1}, which seemingly reflects the formation of microgel-core star polymers and their long-range spatial order. The theoretical analyses of the SANS profiles to be discussed later in sec. 4.2.4 elucidated that the shoulder peak originated from the second-order peak in the structure factor $S(q)$ in eq 16.

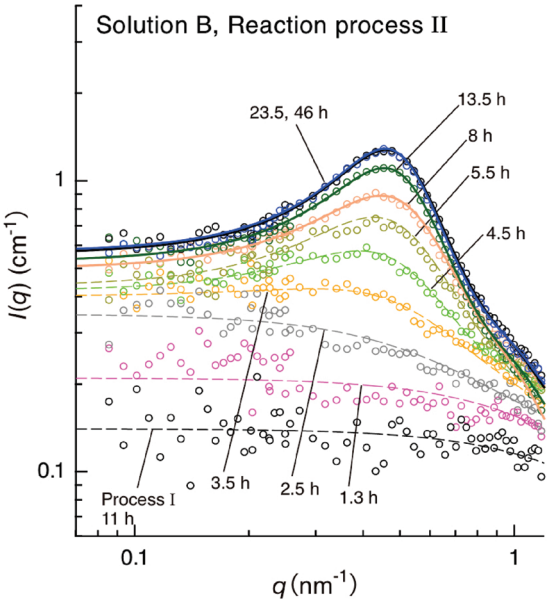

Figure 8. *In situ* and time-resolved SANS profiles of solution B at varying polymerization time t obtained in reaction process II. The profiles shown by circles and solid lines indicate the experimental and theoretical scattering profiles, respectively, where the theoretical scattering profiles at $t \geq 8$ h were reproduced by eq 16. The dashed lines on the SANS profiles are guides for the eyes.

4. Discussion

4.1. Analysis of SANS Profiles in Reaction Process I. In order to quantitatively investigate SANS profiles, we first performed a model analysis according to the following method. In the whole stage of reaction process I, the solution is composed of linear PMMA arms, thereby obeys the OZ formalism for homopolymer solutions:[34]

$$I_{OZ}(q) = I(q = 0)/(1 + \xi^2 q^2) \quad (2)$$

where $I(q = 0)$ and ξ are, respectively, the forward scattering intensity, which depends on the osmotic compressibility of the solution, and the correlation length for the thermal concentration fluctuations of the polymers [PMMA (**2**)] in the solution. In the case of $C/C^* < 1$, ξ is related to the R_g of the swollen polymer chains; $\xi^2 = (R_g^2/3)[(1 - \phi)/(1 - \phi + \phi N_P)]$ with N_p and ϕ being the degree of polymerization of MMA and the volume fraction of the PMMA, respectively, whereas in the case of $C/C^* > 1$, ξ corresponds to a screening length of concentration fluctuations or the so-called concentration-blob size.[36]

SANS profiles in reaction process I were examined on the basis of eq 2. The so-called OZ plot, $1/I(q)$ vs q^2, gave a straight line, enabling us to determine the two characteristic parameters $I(q = 0)$ and ξ at a given t. The solid lines in Figure 7a presents the theoretical profiles obtained by using thus determined $I(q = 0)$ and ξ for reaction process I.

In Figure 9a, thus determined value of ξ and $I(q = 0)$ is plotted together with C/C^* as a function of polymerization time t. The time-dependent value of C/C^* can be evaluated from $C_{MMA}(t)$ and molecular parameters of PMMA (R_g and M_w). Because the concentration of PMMA, $C(t)$, and $C^*(t)$ are calculated by the follow equations,

$$C(t) = C_{MMA}(t)C_{0,MMA}(\rho_{PMMA}/\rho_{MMA}) \quad (3)$$

$$C^*(t) = 3M_n/[4\pi N_A R_g(t)^3] \quad \text{and} \quad R_g(t)^2 = n(t)b^2/6 \quad (4)$$

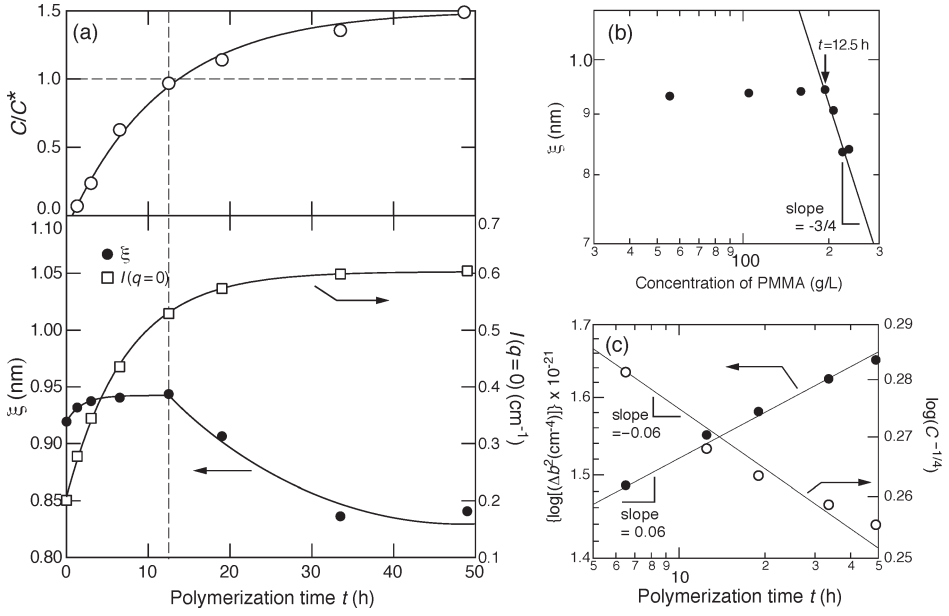

Figure 9. (a) Plots of C/C^* (open circles), correlation length ξ (filled circle), and $I(q = 0)$ (open squares) of solution A in reaction process I as a function of polymerization time t. The vertically and horizontally drawn dashed lines indicate the boundary between the dilute solution ($C/C^* < 1$) and semidilute solution ($C/C^* \geq 1$) of PMMA arms. (b) Double logarithmic plot of the correlation length ξ vs the concentration of PMMA. (c) Plots of $\log(\Delta b^2)$ (filled circles) and $\log(C^{-1/4})$ (open circles) of solution A vs $\log(t)$. The solid lines are guides for the eyes.

where $C_{0,MMA}$, ρ_{PMMA}, and ρ_{MMA} are the initial concentration of MMA monomer (0.198 g/mL), the density of PMMA (1.19), and the density of MMA (0.94), respectively. $n(t)$ and b are the number-average DP obtained by SEC and the segment length of PMMA (0.72 nm),[37] respectively. As the polymerization proceeds from $t = 0$ to 12.5 h in reaction process I where $C/C^* \lesssim 1$, ξ increases, implying that the linear PMMA chains grow in its characteristic length R_g via the living radical polymerization.

The polymerization solution after $t = 12.5$ h satisfied $C/C^* \gtrsim 1$, because over 60% of MMA was converted into PMMA chains to increase C, and C^* decrease with t due to an increase of R_g with t. In this regime, ξ decreases as the polymerization proceeds, even though R_g of a single PMMA chain itself increases. The decrease of ξ with time is a consequence of a decreasing size of the concentration blobs[36] due to increasing c/c^* with time in the context of the scaling theory for the semidilute solutions. According to the scaling theory,[36] ξ is given by

$$\xi(t) \sim C(t)^{-3/4} \tag{5}$$

When ξ vs t is converted to ξ vs C by using C vs t as estimated by eq 3, ξ vs C satisfies the scaling theory of eq 5 in the late stage of reaction process I at $t \gtrsim 12.5$ h, as shown by the solid line in Figure 9b, implying that the propagating PMMA chains form a semidilute solution as predicted by the theory without formation of aggregations.

$I(q = 0)$ is generally given by

$$I(q = 0) \sim \Delta b^2 C / \left(\frac{\partial \Pi}{\partial C}\right) \tag{6}$$

in the context of the fluctuations theory of scattering,[38] where Π is the osmotic pressure and Δb is the scattering contrast difference between solute and solvent which is given by eqs 8 and 9 below. In the semidilute solutions, Π is given by $\Pi \sim C^{9/4}$ and hence

$$I(q = 0) \sim \Delta b^2 C^{-1/4} \tag{7}$$

Thus, if Δb is constant with t, $I(q = 0)$ is expected to decrease with t as C increases with t. On the contrary, the experimental value $I(q = 0)$ is almost constant with t in the semidilute solution regime at $t \gtrsim 12.5$ h. This discrepancy should be attributed to an increase of Δb with t during the polymerization. The solvent for PMMA consists of MMA monomers and toluene-d_8, and MMA monomers are converted to PMMA, which increases the scattering length density of the solvent and hence Δb,

$$\Delta b = b_{solvent} - b_{PMMA} \tag{8}$$

$$b_{solvent} = (1 - \phi_{MMA}) b_{toluene\text{-}d_8} + \phi_{MMA} b_{MMA} \tag{9}$$

where b_J (J = PMMA, MMA, or toluene-d_8) is the scattering length density of the Jth component and ϕ_{MMA} is the volume fraction of MMA monomers in the solvent. Here we should note that the concentration of $RuCl_2(PPh_3)_3$ and n-Bu_3N, which also exist in the matrix medium, is so small that their contributions to $b_{solvent}$ can be neglected. It should be noted that $b_{toluene\text{-}d_8} > b_{MMA}$. As ϕ_{MMA} decreases with t due to the polymerization, $b_{solvent}$ and hence Δb increases with t.

We can calculate Δb and $C^{-1/4}$ as a function of t. The results are shown in Figure 9c. We find the linear relations in $\log(\Delta b^2)$ vs $\log(t)$ and $\log(C^{-1/4})$ vs $\log(t)$ with the slope of $\sim$0.06 and ~ -0.06, respectively. The result actually indicates that Δb^2 increases with t according to $t^{0.06}$ and that this increase in Δb^2 is canceled by the decrease of $C^{-1/4}$ with t according to $t^{-0.06}$. Consequently, we can predict that $I(q = 0)$ is independent of t in reaction process I at $C/C^* > 1$, as found in Figure 9a.

4.2. Analysis of SANS Profiles in Reaction Process II. The addition of the EGDMA solution to the PMMA solution at the beginning of reaction process II is calculated to decrease the polymer concentration C and hence C/C^* down to $\sim$1. In reaction process II, the PMMA chain grows into the block copolymer with the short random copolymer of DP $\sim$ 6.5 as will be detailed below. The block copolymers are then linked into the star polymers. Let us here estimate how much C/C^* will change before and after the linking. If all linear chains in the systems are linked into star polymers having the m arms, and C/C^* before and after the linking are defined by $(C/C^*)_l$ and $(C/C^*)_{star}$, respectively, then the ratio

$$R \equiv (C/C^*)_{star}/(C/C^*)_l = \left(3 - \frac{2}{m}\right)^{3/2}/m \tag{10}$$

This equation is obtained by noting that the radius of gyration of the m-arm star with each arm having the radius of gyration R_g is given by $(3 - 2/m)^{1/2} R_g$ on the basis of the Gaussian chain statistics.[26c] The value R is a maximum at $m = 2$ ($\sim$1.4) and then decreases to zero with m. The value R is about 1 for $m = 3$ and 4. Hence we can predict $C/C^* \lesssim 1$ in the whole reaction process II.

4.2.1. Three Characteristic Reaction Stages in Reaction Process II. The time evolution of the SANS profile as a whole observed in reaction process II may be qualitatively characterized by time evolution of the scattering profiles at the following three representative q-ranges: (i) $I(q = 0)$ at the small q-limit which depends on osmotic compressibility of the systems, where $I(q = 0)$ in reaction process II was assumed to be equal to the scattering intensity at the smallest $q \sim 0.06$ nm^{-1} accessed by our SANS experiment (see Figure 7b), (ii) the q_m value at the scattering maximum, if it exists, as a representative of the scattering in the intermediate q-range, and (iii) the intensity at the high-q limit, $I(q = 1$ nm$^{-1})$ and the exponent α which approximately characterizes the q-dependence of the intensity around the high q limit [$0.8 \lesssim q$ (nm^{-1}) $\lesssim 1.4$] when $I(q)$ is approximated by the power law, $I(q) \sim q^{-\alpha}$. Figures 10a and 10b show the four characteristic scattering parameters as a function of t (part a) and conversion (part b) of the linking agent EGDMA, C_{EGDMA}, where C_{EGDMA}s were determined from the solid line drawn on C_{EGDMA} vs t in Figure 3. The time- and conversion-dependence of these four parameters shown in Figure 10 consistently reveal that the reaction process II can be classified into three characteristic processes, process II-1 to II-3 as also shown in the figure.

In process II-1, $I(q = 0)$ increases as the polymerization proceeds, because the increase of M_w of the reaction products, which is due to both (a) the block copolymerization of EGDMA and MMA and (b) the intermolecular linking reactions to form small star polymers, contributes to increase the osmotic compressibility in the reaction solution. These processes (a and b) in process II-1 as summarized in Scheme 2 also cause enhanced thermal concentration fluctuations so that both the amplitude and thermal correlation length of the fluctuations increase, which in turn increase $I(q = 1$ nm$^{-1})$ and α, respectively.

In process II-2, at $t \cong 10$ h or $C_{EGDMA} \cong 0.5$, $I(q = 0)$ and α (the q-dependence of $I(q)$ at the high q-limit) start to increase abruptly. In the middle of this process, the scattering maximum distinctly appears, and q_m increases rapidly with t or C_{EGDMA}. These results may indicate that the number of star polymers rapidly increases, while the average distance between them rapidly decreases via (a) star−star and (b)

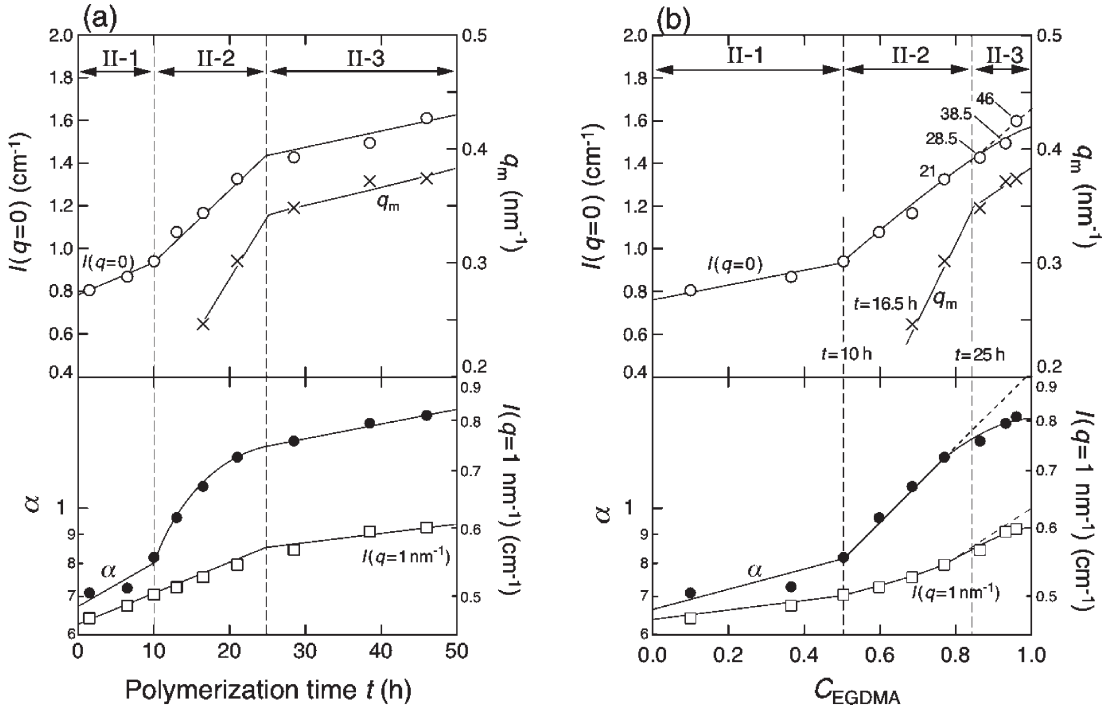

Figure 10. Four characteristic scattering parameters obtained in reaction process II, $I(q = 0)$, q_m, $I(q = 1\ nm^{-1})$, and α as a function of (a) t and (b) C_{EGDMA}. The vertical dashed lines classify reaction process II into three characteristic reaction processes, process II-1 to II-3. The solid lines are guides for the eyes.

Scheme 2. Classification of the Microgel-Core Star Polymer Formation Mechanism via the Arm-Linking Reaction Method, Elucidated by *in Situ* and Time-Resolved SANS and Molecular Analyses (SEC, GC, NMR, and SEC−MALLS)

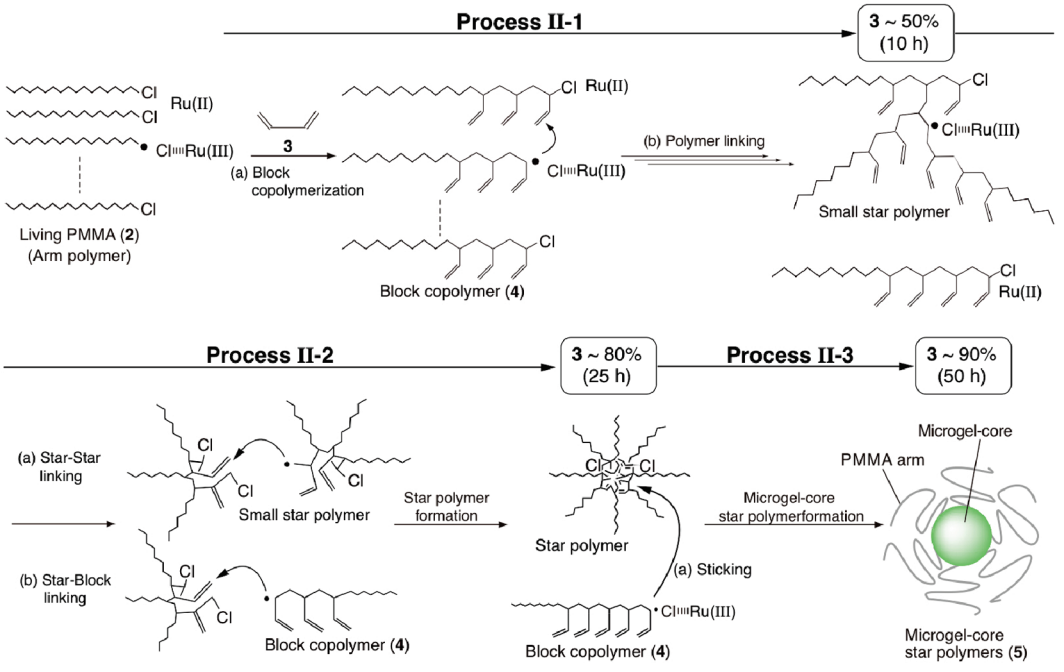

star-block linking reactions in process II-2 as also summarized in Scheme 2.

At $t \gtrsim 25$ h or $C_{EGDMA} \gtrsim 0.84$ in process II-3, all these scattering parameters exhibited a showing down in the rate of increase. This is probably because the microgel-core star polymers are slowly formed via linking of the block copolymer radicals to the star polymers [designated as (a) "sticking" reaction of block copolymers as summarized in process II-3, Scheme 2], and their number slowly increases with t and C_{EGDMA}.

In this work, the time-evolution of the arm number per star polymer, $N_{SEC-MALLS}$, was investigated in the course of reaction process II using SEC−MALLS. $N_{SEC-MALLS}$ was calculated as follows,

$$N_{SEC-MAALS} = w_{PMMA} M_{w,Star-MALLS} / M_{w,Arm-SEC} \quad (11)$$

where w_{PMMA} are weight fraction of the PMMA arm in the star polymer.[32] $M_{w,Star-MALLS}$ and $M_{w,Arm-SEC}$ are weight-average molecular weight of the star polymer or PMMA arm, obtained by SEC−MALLS and SEC, respectively.[16,17]

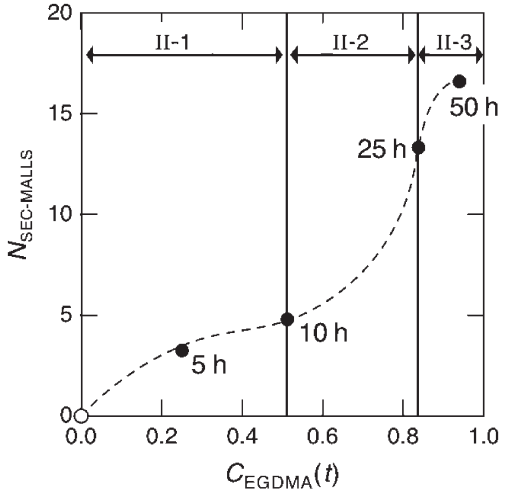

Figure 11. Arm numbers per microgel-core star polymer for solution A evaluated by SEC−MALLS in reaction process II as a function of C_{EGDMA}. The dashed lines are guides for the eyes.

Table 2. Classification of Reaction Process II

Process II-1	(a) block copolymerization
	(b) small star polymer formation (linking reaction)
Process II-2	(a) star−star linking
	(b) star−block linking
Process II-3	(a) sticking of block copolymers into microgel-core star polymers

In Figure 11, $N_{SEC-MALLS}$ thus evaluated was plotted as a function of $C_{EGDMA}(t)$. Although there are only a few data points, the trend of $N_{SEC-MALLS}$ vs C_{EGDMA} is found to be classified into the same three processes, processes II-1 to II-3, such as those found with the SANS method. Moreover, the molecular analysis reveals the followings important facts: Small star polymers with $N_{SEC-MALLS}$ up to ~5 will be formed in process II-1, while the arm numbers per star polymer increases rapidly with C_{EGDMA} in process II-2, and the rate of increase slows down in process II-3.

Table 2 and Scheme 2 summarize the proposed classification of reaction process II. Process II-1 competitively involves (a) block copolymerization of EGDMA and MMA into the arm polymer of PMMA-*block*-Poly(EGDMA-*ran*-MMA) and (b) small star polymer formation (linking reaction) among the arm polymers. In process II-2, (a) a star−star linking reaction and (b) a star−block linking reaction occur to form the star polymers with an increasing number of arm polymers. The process will form the microgel-core star polymers in the late stage of the process. Finally, (a) sticking of linear block copolymers into the microgel-core star polymers may dominantly occur in process II-3. The arm polymers, as many as ~17 attached on the core surface, give rise to entropically driven repulsive interactions among microgel-core star polymers and stabilize the dispersion of them in the solution.

4.2.2. Evaluation of the Volume Fraction of Arm Polymers and Star and/or Microgel-Core Star Polymers for Quantitative SANS Analyses. The analyses in section 4.2.1 elucidated that the reaction system contains the linear arm polymers with weight fraction w_1 and star and/or microgel-core star polymers with weight fraction $w_2 = 1 - w_1$. Quantitative analyses of each fraction is important to characterize the reaction solution with SANS. For the quantitative analyses of w_1 and w_2, the SEC curve at a given t was decomposed into two components as shown in Figure 12a: $f_{Peak\ 1}$ (shown by dotted lines), associated with the linear arms [PMMA and/or PMMA-*block*-poly(EGDMA-*ran*-MMA)], and f_{Peak2} (shown

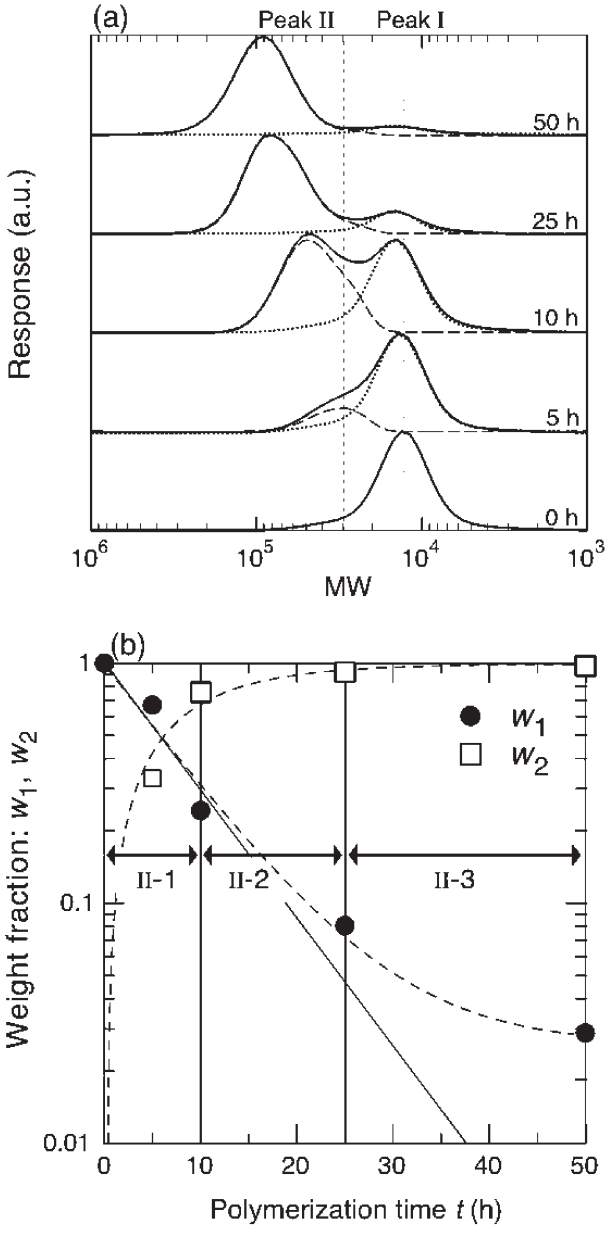

Figure 12. (a) Decomposition of the experimentally observed SEC curves, f_{obs} (solid lines), for solution A in reaction process II at varying polymerization times into the component of the linear arm polymers, $f_{Peak\ I}$ (dotted lines), and the component of the star and/or microgel-core star polymers, $f_{Peak\ II}$ (dashed lines). The vertical dashed lines indicate the peak positions of peaks I and II at a given t. (b) Weight fraction of the linear arm polymers, w_1, and the star and/or microgel-core star polymers, w_2, estimated from the decomposed peak area of peaks I and II, respectively, as a function of the polymerization time t.

by broken lines), associated with the small star polymers, star polymers, and/or microgel-core star polymers. We assumed that $f_{Peak\ 1}$ at a given t is given by the same shape as that at $t = 0$, though the peak position was shifted toward higher molecular weight with t to some extent. For the decomposition, we first estimated $f_{Peak\ 1}$ by best-fitting of $f_{Peak\ 1}$ with the observed curve (f_{obs}) as the peak position and height as adjustable parameters, and $f_{Peak\ 2}$ was then evaluated from $f_{obs} - f_{Peak\ 1} = f_{Peak\ 2}$ at a given t. The time-evolution of w_1 and w_2 were determined from the areas under the peaks for $f_{Peak\ 1}$ and $f_{Peak\ 2}$, and the results are shown in Figure 12b.

We expect that $\log w_1$ should linearly decrease with t along the solid line, as shown in Figure 12b, if the intermolecular linking

reaction of the block copolymers obeys first-order reaction kinetics in reaction process II. It does so in process II-1, but the deviation gradually and increasingly develops with t in processes II-2 and II-3. That attributes to a reaction probability for the intermolecular linking reactions of the block copolymers in processes II-2 and II-3 that decreases with t, because the steric hindrance on the linking reactions increases as the star polymers and/or the microgel-core star polymers become large.

These results shown in Figures 11 and 12 indicate that the solution in process II-1 contains linear arm polymers and small star polymers, while the solution in process II-3 mostly contains microgel-core star polymers with only a minor fraction of linear polymers, the contribution of which to the SANS can be negligible. On the other hand, the solution in reaction process II-2 is quite complex, containing linear polymers, small and large star polymers, and microgel-core star polymers, which makes the SANS analyses impracticable, because too many unknown parameters are involved in the analyses. Hence we shall conduct the analyses only for process II-1 and II-3 below. In order to conduct the SANS analyses in process II-2, we need more data concerning the time-evolution of SEC and SEC−MALLS. This deserves future work.

4.2.3. Analysis of SANS Profiles in Process II-1. The reaction solution is composed of diblock copolymers (**4**) poly(MMA-*ran*-EGDMA), and small star polymers. The scattering length densities of EGDMA (3) and MMA segment are similar and smaller than that of toluene-d_8. Therefore, the scattering from the diblock copolymer (**4**) and the small star polymer is the essentially the same as that from the corresponding homopolymers.

We carried out a theoretical analysis for SANS profiles at $t = 6.5$ and 10 h in process II-1. It is assumed that the form factor of small star polymer, $P_{\mathrm{Star}}(q)$, and block copolymer, $P_{\mathrm{Linear}}(q)$, are given by the Benoit's form factor for the Gaussian n-arm star polymer[39] and the Debye form factor for the Gaussian linear polymer,[40] respectively.

$$P_{\mathrm{Star}}(q) = \frac{2}{N_{\mathrm{SANS}}x^2}\left\{(x-1)+\exp(-x) + \frac{(N_{\mathrm{SANS}}-1)}{2}[1-\exp(-x)]^2\right\} \quad (12)$$

$$P_{\mathrm{Linear}}(q) = \frac{2}{x^2}[x-1+\exp(-x)] \quad (13)$$

Here $x \equiv q^2R_g^2$, and N_{SANS} is the arm-number of the n-arm star polymer. The radius of gyration R_g for the arm polymers and that for the linear polymer were assumed to be identical. We assume no polydispersity with respect to R_g and N_{SANS} for simplicity. In the reaction solution, the small star polymers and the block copolymers exist with weight ratio of w_2/w_1 ($w_2 + w_1 = 1$), evaluated from the SEC analyses (Figure 12). Therefore, the scattering function for the reaction solution in process II-1 is given by

$$I(q) = K[N_{\mathrm{SANS}}w_2P_{\mathrm{Star}}(q) + w_1P_{\mathrm{Linear}}(q)] \quad (14)$$

where K is a proportionality constant which depends on total polymer concentration and M_w of the arm polymers. In Figure 7b, the theoretical profiles based on eq 14 (solid lines) well reproduce the experimentally observed SANS profiles (open circles) at $t = 6.5$ and 10 h. The characteristic parameters, N_{SANS}, R_g, w_1, and w_2, obtained by the best fit, are summarized in Table 3. In this analysis, we used the values w_1 and w_2 shown in Table 3 which were determined from the solid straight line in process II-1in Figure 12b. The values of N_{SANS} thus evaluated at $t = 5$ and 10 h are slightly smaller than those of $N_{\mathrm{SEC-MALLS}}$ shown in Figure 11. It is noted that the size of core can be regarded as zero in this model analysis in process II-1.

Table 3. Summary of Characteristic Parameters Determined by the *In Situ* and Time-Resolved SANS for Solution A at $t = 6.5$ and 10 h (Process II-1)

t (h)	6.5	10
N_{SANS}	2.4 ± 0.3	3.6 ± 0.3
R_g (nm)	1.5 ± 0.2	1.6 ± 0.2
w_1	0.33	0.21
w_2	0.67	0.79

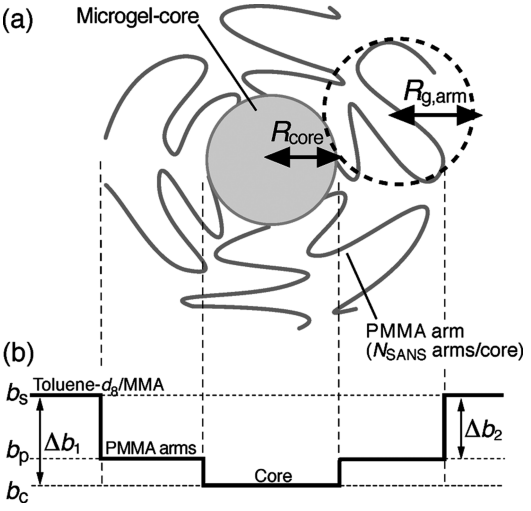

Figure 13. (a) Schematic illustration of the microgel-core star polymer, and (b) the relative scattering length densities of the matrix (toluene-d_8/MMA), the PMMA arms, and the core.

4.2.4. Analysis of SANS Profiles in Process II-3. Here, we carried out the theoretical analysis of the SANS profiles in process II-3 in order to characterize the microgel-core structure. We assumed a scattering model function, which is composed of the two contributions: thermal concentration fluctuations of the block copolymers, $I_{OZ}(q)$, and the microgel-core star polymers $I_{\mathrm{mgstar}}(q)$, as follows,

$$I(q) = w_1I_{OZ}(q) + w_2I_{\mathrm{mgstar}}(q) \quad (15)$$

The coefficients (w_1 and w_2) of the first and second term were evaluated from the corresponding broken lines shown in Figure 12b, though the contribution of the first term is negligibly small. $I_{\mathrm{mgstar}}(q)$ is given by a product of the form factor of the microgel-core, $P_{\mathrm{mgstar}}(q)$, and the structure factor $S(q)$,

$$I_{\mathrm{mgstar}}(q) = nP_{\mathrm{mgstar}}(q)S(q) \quad (16)$$

where n is the number density of microgel-core star polymers. For $P_{\mathrm{mgstar}}(q)$, we employed a core−shell sphere model proposed by Pedersen et al. (see Appendix).[41] As illustrated in Figure 13a, the model assumes that (i) the shell and microgel-core are, respectively, composed of the PMMA arms and poly(MMA-*ran*-EGDMA) copolymers, both swollen by toluene-d_8, as a good solvent; (ii) one chain end of PMMA arms is anchored on the surface of the microgel-core; (iii) PMMA arms in the shell do not penetrate into the swollen micogel-core. Here, three parameters were introduced in order to characterize the structure of the single microgel-core star polymer; core size (R_{core}), radius of gyration of PMMA arms in the shell ($R_{g,\mathrm{arm}}$), and the number of PMMA arms emanating from the single microgel-core (N_{SANS}), which will be introduced later. In this analysis, we neglected the polydispersity for R_{core}, $R_{g,\mathrm{arm}}$, and N_{SANS}, for

Table 4. Summary of Characteristic Parameters Determined by the *In Situ* and Time-Resolved SANS for Solution A at $t \geq 28.5$ h (Process II-3) and for Solution B at $t \geq 8$ h

	solution A			solution B			
t (h)	28.5	38.5	46.6	8	13.5	23.5	46
N_{SANS}	12.7 ± 0.5	15.1 ± 0.6	18.2 ± 0.7	8.5 ± 0.5	11.9 ± 0.6	16.1 ± 0.5	16.6 ± 0.5
R_{core} (nm)	0.8 ± 0.1	0.9 ± 0.2	1.0 ± 0.2	0.7 ± 0.2	0.8 ± 0.1	0.9 ± 0.1	0.9 ± 0.1
$R_{g,arm}$ (nm)	2.0 ± 0.2	2.0 ± 0.1	2.0 ± 0.1	1.6 ± 0.1	1.8 ± 0.1	1.8 ± 0.1	1.8 ± 0.1
R_h (nm)	6.0 ± 0.3	6.3 ± 0.3	6.4 ± 0.3	5.6 ± 0.2	5.8 ± 0.2	5.9 ± 0.3	5.9 ± 0.3
n ($cm^{-3} \times 10^{17}$)	3.6 ± 0.5	3.5 ± 0.4	3.5 ± 0.4	6.8 ± 0.5	6.6 ± 0.4	6.4 ± 0.3	6.4 ± 0.3
η	0.10 ± 0.01	0.12 ± 0.01	0.13 ± 0.01	0.14 ± 0.01	0.17 ± 0.02	0.18 ± 0.02	0.19 ± 0.02

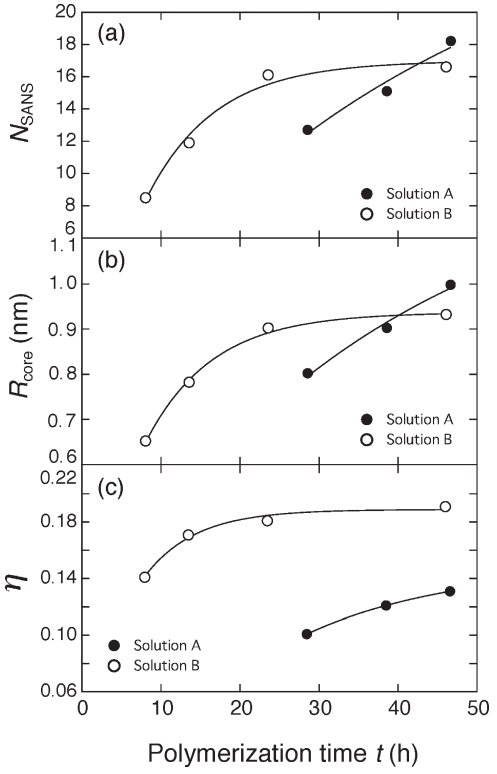

Figure 14. Summary of the polymerization-time dependence of the characteristic parameters (process II-3) obtained by quantitative analyses for the SANS profiles for solution A at $t \geq 28.5$ h (filled circles) and for solution B at $t \geq 8$ h (open circles). (a) N_{SANS}, (b) R_{core}, (c) η. The solid lines are guides for the eyes.

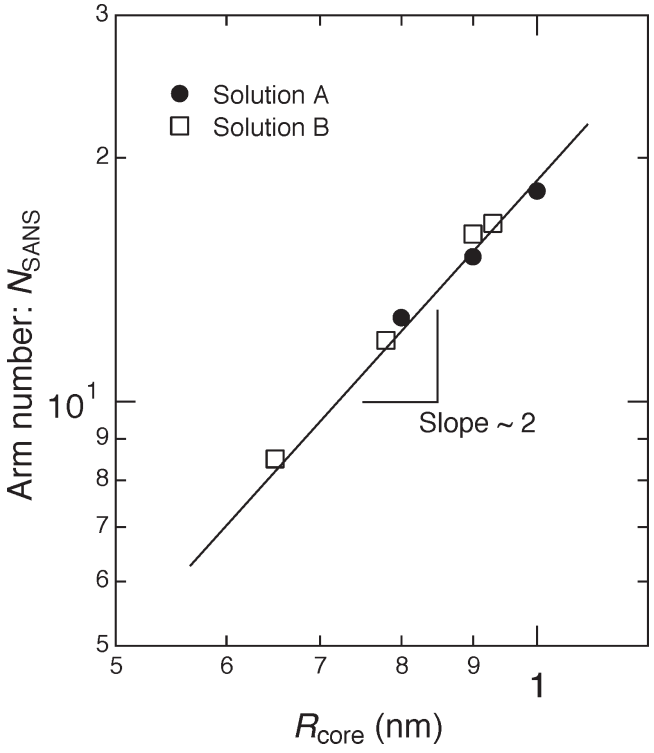

Figure 15. Arm numbers N_{SANS} per a single microgel-core star polymer vs average core radius R_{core} as determined from SANS.

simplicity. Figure 13b schematically illustrates the spatial distribution of the scattering contrast, Δb_1 and Δb_2, across the microgel-core star polymer.

As for $S(q)$, which originates from the interactions among microgel-core star polymers, we employed the hard sphere model given by Percus−Yevick formalism.[42] In this model, we replace the microgel-core star polymers by equivalent hard spheres of radius R_h, which have an excluded volume given by the sphere of radius $L = 2R_h$, and volume fraction η (see Appendix).

4.2.5. Characterization of Microgel-Core Star Polymers. The solid lines in Figures 7b (drawn for the SANS profiles for solution A obtained at polymerization time $t \gtrsim 25$ h) and Figure 8 (drawn for those for solution B obtained at $t \gtrsim 4.5$ h) show the theoretical scattering curves best-fitted with the experimental profiles (open circles) using eq 16. Time-evolution of the characteristic parameters, N_{SANS}, R_{core}, $R_{g,arm}$, R_h, n, and η, obtained for both solution A and B in reaction process II are summarized in Table 4. In the determination of n, we took into account the change of the scattering length density of the solvent with time during the polymerization process, as discussed earlier in conjunction with eqs 8 and 9. Moreover, some of these characteristic parameters for solution A and B were plotted in Figures 14a-c as a function of t. As for solution B, we presented the characteristic parameters obtained at $t \gtrsim 8$ h, where the solution exhibited the macroscopic gelation. In both solutions A and B, N_{SANS} and R_{core} at the end of reaction process II are close to ~18 and ~1 nm, respectively (see Figure 14, parts a and b). However, in solution B, a microgel-core star polymer grows more rapidly as compared to that in solution A. The final value of $N_{SANS} \sim 18$ agrees well with the independent estimation by SEC−MALLS ($N_{SEC-MALLS} = 17$).[16a,b,d,e,17] In both solution A and B, we found that N_{SANS} increased in proportion to R_{core}^2, as will be shown below in Figure 15, implying that a single arm polymer occupies the given surface area of the micogel-core independent of t in process II-3. The $R_{g,arm}$, estimated for both solutions A and B, is almost constant at ~2.0 and ~1.8 nm, respectively. In process II-3 for both solutions A and B, n and R_h are nearly constant as shown in Table 4, respectively. The slight increase of η ($\propto nR_h^3$) with t in solution A and B can be accounted for by the small changes in n and R_h with t.

4.3. Mechanism for Reaction Process II. By comparing the results obtained from the model analysis of the time-resolved SANS profiles and those from the molecular characterization by SEC and NMR, we shall discuss the mechanism in linking reaction process II with respect to the following three

processes: (1) the competition between diblock copolymerization and small star polymer formation (process II-1), (2) microgel-core star polymer formation (processes II-2 and II-3), and (3) macroscopic gelation.

4.3.1. Competing Reaction of Diblock Copolymerization and Small Star Polymer Formation in Process II-1. After *in situ* addition of EGDMA (**3**) into solution A, the molar ratio between residual MMA and EGDMA (**3**) was close to 1/1 with about 90% conversion of MMA. Therefore, 5 h after the addition, the random copolymerization between MMA and EGDMA occurred from the terminal of living prepoly(MMA) arms (**2**), yielding block copolymers (**4**) consisting of a PMMA and a short random copolymers of MMA and EGDMA, as shown in Peak I of SEC (Figure 4b). The apparent molecular weight of block copolymer $M_{app,I}$ reached a constant value of 970 at the end of process II-1, and hereafter $M_{app,I}$ was independent of C_{total}. The structure of the block copolymers carrying unreacted vinyl pendants are also supported by the ^{1}H NMR analysis (Figure 6). Simultaneously, a small shoulder peak II at the higher molecular weight (see Figure 4b at $t = 5$ h; yield $\sim 20\%$) also appeared, corresponding to the small star polymer (dimer or trimmer of the diblock polymers, linked via dangling vinyl groups). Up to $t = 10$ h (process II-1), peak II increases and shifts toward higher molecular weight side (yield $\sim 55\%$), which is consistent with the time-resolved SANS analysis (Figure 10a). SANS profiles obtained at $t = 6.5$ and 10 h for solution A can be well reproduced by the composite model of the *n*-arm star polymer and the linear polymer given by eq 14, with the number of the arms in the star polymers N_{SANS} increased up to $\sim$4 (Table 3), consistent with the results of the molecular characterization with SEC−MALLS (Figure 11). These results clearly elucidated that process II-1 involved the two competing reactions as indicated in Scheme 2 and Table 2: (i) diblock copolymerization [process II-1(a)] and (ii) the small star polymer formation via polymer linking [process II-1(b)]. Process II-1 commonly occurs for both solution A and B, though the reaction rate is different between these solutions; in case of solution B, process II-1 appeared at $t < 3.5$ h.

4.3.2. Microgel-Core Star Polymer Formation. The time-resolved SANS profiles obtained in reaction process II for solution A exhibit a scattering maximum at $t \gtrsim 16.5$ h (Figures 7b and 10a). The maximum is possibly interpreted to arise from the excluded volume effects as described by Percus−Yevick type hard spheres.[42] The excluded volume effects are anticipated to be effective when the sizable hard microgel-core are developed in the star polymers, while they are not so when the core is small and relatively flexible as in the case of the small star polymers and the star polymers in process II-2 in Scheme 2. From this viewpoint, the time-resolved SANS quantitatively elucidates the time-evolution of the microgel-core star polymer formation and its spatial distribution of them in the time range of $25 \lesssim t$ (h) $\lesssim 46$. The analyses of the time-resolved SANS based on the core−shell model yielded the following pieces of information: (i) the number density of the microgel-core stars *n* is nearly constant, as shown in Table 4; (ii) however, N_{SANS} and R_{core} for solution A and B continue to increase in process II-3 except at t $\gtrsim$ 23.5 h for solution B where the reaction appears to be completed (see Figures 14a and b). Considerations i and ii suggest that the sticking of the linear block copolymers into the star polymer dominantly occurs in process II-3(a), as summarized in Scheme 2 and Table 2.

4.4. Macroscopic Gelation. The macroscopic gelation was found to occur at $t \geq 8$ h in reaction process II for solution B, based on the fact that the gel never flowed and was never dissolved by solvents. Why did the gel form only in solution B? We can find the following factors in Figure 14. (i) $R_{core}^2/N_{SANS} \sim 0.05$ nm^2 independent of *t* for both solution A and solution B as shown in Figure 15, suggesting that the core surfaces developed in both solutions are equally covered by the PMMA brush chains and hence are subjected to about equal entropic repulsion against neighboring core surfaces; (ii) the volume fraction of the hard spheres η equivalent to the microgel-core star polymers for solution B is larger than that for solution A by a factor of $\sim$1.4 to $\sim$2.0, suggesting that the average distance between the cores is closer in solution B than in solution A.

Factors (i) and (ii) enable the cores in the solution B to approach one another more closely than those in solution A, driven by thermal fluctuations, so that they are more likely to be chemically connected via the linking reaction into a macroscopically percolated networks. It is crucial to conduct ultrasmall angle neutron scattering (USANS) experiments which cover $q < 0.1$ nm^{-1} in order to explore the percolated network structures and its heterogeneities extending over a length scale larger than that covered by SANS. This deserves future work.

5. Conclusion

We employed in situ and time-resolved SANS measurements, in conjunction with GC, SEC, and ^{1}H NMR analyses, to elucidate kinetic pathways of the formation of the microgel-core star polymers via Ru(II)-catalyzed living radical polymerization. The synthetic process analyzed by the time-resolved SANS method included the following two processes: (1) synthesis of the linear arm polymers (reaction process I); (2) linking reaction of the linear arm polymers with a divinyl compound [reaction process II]. The SANS profiles in the reaction process II were quantitatively analyzed on the basis of the models of the *n*-arm star polymers and the microgel-core star polymers, described in the text. As a result, the mechanism of arm-linking reaction was summarized by the three steps as visualized in Scheme 2 in the text.

Appendix

1. Core−Shell Spherical Model. On the basis of the core-shell model shown in Figure 13,[41] the form factor of a single microgel-core star polymer, $P_{mgstar}(q)$, is composed of four partial scattering functions: $F_c(q)$ for a microgel-core, $F_a(q)$ for a single arm polymer, and cross-terms between microgel-core and arm polymer, $S_{ca}(q)$, and between different arm polymers, $S_{aa}(q)$

$$P_{mgstar}(q) = N_{SANS}{}^2 l_c{}^2 F_c(q) + N l_a{}^2 F_a(q) + 2N^2 l_c l_a S_{ca}(q) + N(N-1) l_a{}^2 S_{aa}(q) \quad \text{(A-1)}$$

where N_{SANS} is number of arm polymers anchored on the microgel-core, l_c and l_a are averaged scattering lengths per chain in the microgel-core and arm polymer, respectively, excess to the scattering length of solvent. They can be calculated as $l_c = V_c(b_{solv} - b_c)$ and $l_a = V_a(b_{solv} - b_a)$, respectively, where V_c and V_a are the volume of a single chain [poly(MMA-*ran*-EGDMA)] in the microgel-core and the volume of a single arm polymer (PMMA). b_c and b_a are the corresponding scattering length densities and b_{solv} is the scattering length density of the solvent composed of toluene-d_8 and MMA. Δb_1 and Δb_2 shown in Figure 13(b) are the differences in the scattering densities between the solvent and core and between the solvent and the arm, respectively. $F_c(q)$ for the single microgel-core which is assumed to be uniform is given by

$$F_c(q) = \Phi^2(u), \quad u = qR_{core} \quad \text{(A-2)}$$

and

$$\Phi(u) = 3[\sin(u) - u\sin(u)]/u^3 \quad \text{(A-3)}$$

where R_{core} is radius of the micro-gel core. As for the $F_a(q)$, we assume the Debye function[43] for an ideal Gaussian chain, even though the arm polymer is perturbed by one end being anchored on the microgel-core and by interactions with neighboring arm chains and solvent,

$$F_a(q) = 2[\exp(-x) - 1 + x]/x^2, \quad x = (qR_{g,arm})^2 \quad \text{(A-4)}$$

where $R_{g,arm}$ is the radius of gyration of the arm chain.

In order to avoid penetration of the arm chains against the microgel-core, one end of the arm polymer chain is assumed to start at a distance $R_{core} + R_{g,arm}$ from the center of the microgel-core.[41] Then $S_{ca}(q)$ is given by

$$S_{ca}(q) = \Phi(u)\phi(x)\frac{\sin(u+x)}{u+x} \quad \text{(A-5)}$$

In eq A-5, $\phi(x)[\sin(u+x)]/(u+x)$ is the scattering amplitude for a Gaussian chain,[44] with one end fixed on the surface of the sphere with a radius $R_{core} + R_{g,arm}$, where

$$\phi(x) = [1 - \exp(-x)]/x \quad \text{(A-6)}$$

The partial scattering function $S_{aa}(q)$ for the cross-correlation of the arm polymer chains emanating from surface of microgel-core is given by

$$S_{aa}(u) = \phi^2(x)\left[\frac{\sin(u+x)}{u+x}\right]^2 \quad \text{(A-7)}$$

In order to calculate $S(q)$, we employ the Percus−Yevick model,[42] which incorporates a hard-sphere potential between spheres in liquid-like packing, by replacing the microgel-core with an equivalent hard sphere of radius R_h.

$$S(q) = [1+24\eta G(y)/y]^{-1} \quad \text{(A-8)}$$

where $y = 2qR_h$, R_h, and η are the radius and the volume fraction of the hard sphere, and $G(y)$ is given by

$$\begin{aligned} G(y) = {} & (\alpha/y^2)[\sin(y) - y\cos(y)] + (\beta/y^3)[2y\sin(y) \\ & + (2-y^2)\cos(y) - 2] + (\gamma/y^5)[-y^4\cos(y) \\ & + 4\{(3y^2-6)\cos(y) + (y^3-6y)\sin(y) + 6\}]. \end{aligned} \quad \text{(A-9)}$$

The quantities α, β, and γ are

$$\alpha = (1+2\eta)^2/(1-\eta)^4 \quad \text{(A-10)}$$

$$\beta = -6\eta[(1+(\eta/2)]^2/(1-\eta)^4 \quad \text{(A-11)}$$

$$\gamma = \alpha\eta/2 \quad \text{(A-12)}$$

The shortest distance, L, between the centers of adjacent microgel-cores is given by $L = 2R_h$ in this hard sphere model.

References and Notes

(1) This work was presented in part at the following meeting: (a) The 55th Annual Meeting on the Society of Polymer Science, Nagoya, Japan, May 2006; paper 2C22: Terashima, T.; Motokawa, R.; Kamigaito, M.; Sawamoto, M.; Koizumi, S.; Hashimoto, T. *Polym. Prepr. Jpn.* **2006**, *55*, 171. (b) The 55th Annual Meeting on the Society of Polymer Science, Nagoya, Japan, May 2006; paper 2C23: Motokawa, R.; Terashima, T.; Kamigaito, M.; Sawamoto, M.; Koizumi, S.; Hashimoto, T. *Polym. Prepr. Jpn.* **2006**, *55*, 172. (c) The VIII International Conference on Small-angle Scattering, Kyoto, Japan, July 2006; paper PO-P041b: Terashima, T.; Motokawa, R.; Kamigaito, M.; Sawamoto, M.; Koizumi, S.; Hashimoto, T. (d) The 55th Symposium on Macromolecules, Toyama, Japan, September 2006; paper 2B15: Motokawa, R.; Terashima, T.; Kamigaito, M.; Sawamoto, M.; Koizumi, S.; Hashimoto, T. *Polym. Prepr. Jpn.* **2006**, *55*, 2453–2454.

(2) For reviews on synthesis and properties of star polymers, see: (a) Bauer, B. J.; Fetters, L. *J. Rubber Chem. Technol.* **1978**, *51*, 406–436. (b) Bywater, S. *Adv. Polym. Sci.* **1979**, *30*, 90–116.

(3) For reviews on synthesis of star polymers by living anionic polymerization, see: (a) Hadjichristidis, N. *J. Polym. Sci., Part A: Polym. Chem.* **1999**, *37*, 857–871. (b) Hirao, A.; Hayashi, M.; Loykulnant, S.; Sugiyama, K.; Ryu, S. W.; Haraguchi, N.; Matsuo, A.; Higashihara, T. *Prog. Polym. Sci.* **2005**, *30*, 111–182.

(4) For reviews on synthesis of star polymers by living radical polymerization, see: (a) Gao, H.; Matyjaszewski, K. *Prog. Polym. Sci.* **2009**, *34*, 317–350. (b) Blencowe, A.; Tan, J. F.; Goh, T. K.; Qiao, G. G. *Polymer* **2009**, *50*, 5–32.

(5) Hsieh, H. L.; Quirk, R. P., Ed. *Anionic Polymerization*; Marcel Dekker, Inc.: New York, 1996.

(6) (a) Sawamoto, M. *Prog. Polym. Sci.* **1991**, *16*, 111–172. (b) Matyjaszewski, K., Ed.; *Cationic Polymerization*; Marcel Dekker, Inc.: New York, 1996. (c) Aoshima, S.; yoshida, T.; Kanazawa, A.; Kanaoka, S. *J. Polym. Sci., Part A: Polym. Chem.* **2007**, *45*, 1801–1813.

(7) (a) Kamigaito, M.; Ando, T.; Sawamoto, M. *Chem. Rev.* **2001**, *101*, 3689–3745. (b) Kamigaito, M.; Ando, T.; Sawamoto, M. *Chem. Rec.* **2004**, *4*, 3661–3681. (c) Ouchi, M.; Terashima, T.; Sawamoto, M. *Acc. Chem. Res.* **2008**, *41*, 1120–1132. (d) Ouchi, M.; Terashima, T.; Sawamoto, M. *Chem. Rev.* **2009**, *109*, 4963–5050.

(8) (a) Matyjaszewski, K.; Xia, J. *Chem. Rev.* **2001**, *101*, 2921–2990. (b) Coessens, V.; Pintauer, T.; Matyjaszewski, K. *Prog. Polym. Sci.* **2001**, *26*, 337–377. (c) Tsarevsky, N. V.; Matyjaszewski, K. *Chem. Rev.* **2007**, *101*, 2270–2299. (d) Pintauer, T.; Matyjaszewski, K. *Chem. Soc. Rev.* **2008**, *37*, 1087–1097. (e) Matyjaszewski, K.; Tsarevsky, N. V. *Nature Chem.* **2009**, *1*, 276–288.

(9) Hawker, C. J.; Bosman, A. W.; Harth, E. *Chem. Rev.* **2001**, *101*, 3661–3688.

(10) Moad, G.; Rizzardo, E.; Thang, S. H. *Polymer* **2008**, *49*, 1079–1131.

(11) (a) Zilliox, J.-G.; Rempp, P.; Parrod, J. *J. Polym. Sci., Part C* **1968**, *22*, 145–156. (b) Tsitsilianis, C.; Chaumont, P.; Rempp, P. *Makromol. Chem.* **1990**, *191*, 2319–2328. (c) Tsitsilianis, C.; Graff, S.; Rempp, P. *Eur. Polym. J.* **1991**, *27*, 243–246.

(12) (a) Bi, L.-K.; Fetters, L. J. *Macromolecules* **1976**, *9*, 732–742. (b) Young, R. N.; Fetters, L. J. *Macromolecules* **1978**, *11*, 899–904.

(13) Masuda, T.; Ohta, Y.; Yamauchi, T.; Onogi, S. *Polym. J.* **1984**, *16*, 273–291.

(14) Worsfold, D. J. *Macromolecules* **1970**, *3*, 514–517.

(15) (a) Kanaoka, S.; Sawamoto, M.; Higashimura, T. *Macromolecules* **1991**, *24*, 5741–5745. (b) Kanaoka, S.; Sawamoto, M.; Higashimura, T. *Macromolecules* **1992**, *25*, 6407–6413. (c) Kanaoka, S.; Sawamoto, M.; Higashimura, T. *Macromolecules* **1993**, *26*, 254–259. (d) Shibata, T.; Kanaoka, S.; Aoshima, S. *J. Am. Chem. Soc.* **2006**, *128*, 7497–7504. (e) Kanaoka, S.; Yagi, N.; Fukuyama, Y.; Aoshima, S.; Tsunoyama, H.; Tsukuda, T.; Sakurai, H. *J. Am. Chem. Soc.* **2007**, *129*, 12060–12061.

(16) (a) Baek, K.-Y.; Kamigaito, M.; Sawamoto, M. *Macromolecules* **2001**, *34*, 215–221. (b) Baek, K.-Y.; Kamigaito, M.; Sawamoto, M. *Macromolecules* **2001**, *34*, 7629–7635. (c) Baek, K.-Y.; Kamigaito, M.; Sawamoto, M. *J. Polym. Sci., Part A: Polym. Chem.* **2002**, *40*, 633–641. (d) Baek, K.-Y.; Kamigaito, M.; Sawamoto, M. *J. Polym. Sci., Part A: Polym. Chem.* **2002**, *40*, 1972–1982. (e) Baek, K.-Y.; Kamigaito, M.; Sawamoto, M. *J. Polym. Sci., Part A: Polym. Chem.* **2002**, *40*, 2245–2255.

(17) (a) Terashima, T.; Kamigaito, M.; Baek, K.-Y.; Ando, T.; Sawamoto, M. *J. Am. Chem. Soc.* **2003**, *125*, 5288–5289. (b) Terashima, T.; Ouchi, M.; Ando, T.; Sawamoto, M.; Kamigaito, M. *J. Polym. Sci., Part A: Polym. Chem.* **2006**, *44*, 4966–4980. (c) Terashima, T.; Ouchi, M.; Ando, T.; Sawamoto, M.; Kamigaito, M. *Macromolecules* **2007**, *40*, 3581–3588. (d) Terashima, T.; Ouchi, M.; Ando, T.; Sawamoto, M. *J. Polym. Sci., Part A: Polym. Chem.* **2010**, *48*, 373–379.

(18) (a) Xia, J.; Zhang, X.; Matyjaszewski, K. *Macromolecules* **1999**, *32*, 4482–4484. (b) Gao, H.; Tsarevsky, N.; Matyjaszewski, K. *Macromolecules* **2005**, *38*, 5995–6004. (c) Gao, H.; Matyjaszewski, K. *J. Am. Chem. Soc.* **2007**, *129*, 11828–11834. (d) Ohno, S.; Gao, H.; Cusick, B.; Kowalewski, T.; Matyjaszewski, K. *Macromol. Chem. Phys.* **2009**, *210*, 421–430.

(19) (a) Bosman, A. W.; Heumann, A.; Klaerner, G.; Benoit, D.; Fréchet, J. M. J.; Hawker, C. J. *J. Am. Chem. Soc.* **2001**, *123*, 6461–6462. (b) Bosman, A. W.; Vestberg, R.; Heumann, A.; Fréchet, J. M. J.; Hawker, C. J. *J. Am. Chem. Soc.* **2003**, *125*, 715–728. (c) Helms, B.; Guillaudeu, S. J.; Xie, Y.; McMurdo, M.; Hawker, C. J.; Fréchet, J. M. J. *Angew. Chem., Int. Ed.* **2005**, *44*, 6384–6387. (d) Chi, Y.; Scroggins, S. T.; Fréchet, J. M. J. *J. Am. Chem. Soc.* **2008**, *130*, 6322–6323.
(20) Kato, M.; Kamigaito, M.; Sawamoto, M.; Higashimura, T. *Macromolecules* **1995**, *28*, 1721–1723.
(21) (a) Senoo, M.; Kotani, Y.; Kamigaito, M.; Sawamoto, M. *Macromolecules* **1999**, *32*, 8005–8009. (b) Senoo, M.; Kotani, Y.; Kamigaito, M.; Sawamoto, M. *Macromol. Symp.* **2000**, *157*, 193–200.
(22) Fuji, Y.; Watanabe, K.; Baek, K.-Y.; Kamigaito, M.; Sawamoto, M. *J. Polym. Sci., Part A: Polym. Chem.* **2002**, *40*, 2055–2065.
(23) Nakatani, K.; Terashima, T.; Sawamoto, M. *J. Am. Chem. Soc.* **2009**, *131*, 13600–13601.
(24) Yoda, H.; Nakatani, K.; Terashima, T.; Ouchi, M.; Sawamoto, M. *Macromolecules* **2010**, in press.
(25) Baek, K.-Y.; Kamigaito, M.; Sawamoto, M. *Macromolecules* **2002**, *35*, 1493–1498.
(26) (a) Yamauchi, K.; Hasegawa, H.; Hashimoto, T.; Tanaka, H.; Motokawa, R.; Koizumi, S. *Macromolecules* **2006**, *39*, 4531–4539. (b) Miyamoto, N.; Yamauchi, K.; Hasegawa, H.; Hashimoto, T.; Koizumi, S. *Physica B* **2006**, *385*, 752–755. (c) Zhao, Y.; Tanaka, H.; Miyamoto, N.; Koizumi, S.; Hashimoto, T. *Macromolecules* **2009**, *42*, 1739–1748. (d) Zhao, Y.; Miyamoto, N.; Koizumi, S.; Hashimoto, T. *Macromolecules* **2010**, *43*, 2948–2959.
(27) (a) Motokawa, R.; Koizumi, S.; Hashimoto, T.; Annaka, M. *Physica B* **2006**, *385*−*386*, 780–782. (b) Motokawa, R.; Koizumi, S.; Zhao, Y.; Hashimoto, T. *J. Appl. Crystallogr.* **2007**, *40*, s645–s649. (c) Motokawa, R.; Koizumi, S.; Hashimoto, T.; Annaka, M.; Nakahira, T. *Macromolecules* **2010**, *43*, 752–764.
(28) (a) Fetters, L. J.; Balsara, N. P.; Huang, J. S.; Jeon, H. S.; Almdal, K.; Lin, M. Y. *Macromolecules* **1995**, *28*, 4996–5005. (b) Stellbrink, J.; Willner, L.; Jucknischke, O.; Richter, D.; Linder, P.; Fetters, L. J.; Huang, J. S. *Macromolecules* **1998**, *31*, 4189–4197. (c) Stellbrink, J.; Allgaier, J.; Willner, L.; Richter, D.; Slawecki, T.; Fetters, L. J. *Polymer* **2002**, *43*, 7101–7109.
(29) Baek, K.-Y.; Kamigaito, M.; Sawamoto, M. *J. Polym. Sci., Part A: Polym. Chem.* **2002**, *40*, 1937–1944.
(30) Hamasaki, S.; Kamigaito, M.; Sawamoto, M. *Macromolecules* **2002**, *35*, 2934–2940.
(31) (a) Koizumi, S.; Iwase, H.; Suzuki, J.-I.; Oku, T.; Motokawa, R.; Sasao, H.; Tanaka, H.; Yamaguchi, D.; Shimizu, H. M.; Hashimoto, T. *Physica B* **2006**, *385*−*386*, 1000–1006. (b) Koizumi, S.; Iwase, H.; Suzuki, J.-I.; Oku, T.; Motokawa, R.; Sasao, H.; Tanaka, H.; Yamaguchi, D.; Shimizu, H. M.; Hashimoto, T. *J. Appl. Crystallogr.* **2007**, *40*, s474–s479.
(32) See eq 11. w_{PMMA} is calculated from the monomer feed ratio of MMA and **3** and the monomer conversion.
(33) Terashima, T.; Ouchi, M.; Ando, T.; Sawamoto, M. *J. Am. Chem. Soc.* **2006**, *128*, 11014–11015.
(34) Ornstein, L. S.; Zernike, F. *Proc. Akad. Sci. Amsterdam* **1914**, *17*, 793–806.
(35) Flory, P. *Principles of Polymer Chemistry*; Cornell University Press: Ithaca, NY, 1971, Chapter XII.
(36) deGennes, P. G. *Scaling Concepts in Polymer Physics*; Cornell University Press: Ithaca, NY, 1979.
(37) Russell, T. P.; Hjelm, R. P.; Seeger, P. A. *Macromolecules* **1990**, *23*, 890–893.
(38) Debye, P. *J. Appl. Phys.* **1944**, *15*, 338–342.
(39) Benoit, H. *J. Polym. Sci.* **1953**, *11*, 507–510.
(40) Debye, P. *J. Chem. Phys.* **1946**, *14*, 636–639.
(41) (a) Pedersen, J. S.; Gerstenberg, M. C. *Macromolecules* **1996**, *29*, 1363–1365. (b) Pedersen, J. S. *J. Appl. Crystallogr.* **2000**, *33*, 637–640. (c) Pedersen, J. S. *J. Chem. Phys.* **2001**, *114*, 2839–2846. (d) Sommer, C.; Pedersen, J. S. *Langmuir* **2005**, *21*, 2137–2149.
(42) Percus, J. K.; Yevick, G. *Phys. Rev.* **1958**, *110*, 1–13.
(43) Debye, P. *J. Phys. Chem.* **1947**, *51*, 18–32.
(44) Hammouda, B. *J. Polym. Sci., Part B: Polym. Phys.* **1992**, *30*, 1387–1390.